MISCELLANEOUS PAPER N-76-10

CORRELATION OF IMPACT AND EXPLOSIVELY CREATED GROUND SHOCK PHENOMENA

by

Max B. Ford

Weapons Effects Laboratory
U. S. Army Engineer Waterways Experiment Station
P. O. Box 631, Vicksburg, Miss. 39180

June 1976
Final Report

Prepared for Office, Chief of Engineers, U. S. Army
Washington, D. C. 20314

Under Project No. 4A061101A91D

Unclassified

SECURITY CLASSIFICATION OF THIS PAGE (When Data Entered)

REPORT DOCUMENTATION PAGE

READ INSTRUCTIONS BEFORE COMPLETING FORM

1. REPORT NUMBER: Miscellaneous Paper N-76-10
2. GOVT ACCESSION NO.
3. RECIPIENT'S CATALOG NUMBER
4. TITLE (and Subtitle): CORRELATION OF IMPACT AND EXPLOSIVELY CREATED GROUND SHOCK PHENOMENA
5. TYPE OF REPORT & PERIOD COVERED: Final report
6. PERFORMING ORG. REPORT NUMBER
7. AUTHOR(s): Max B. Ford
8. CONTRACT OR GRANT NUMBER(s)
9. PERFORMING ORGANIZATION NAME AND ADDRESS: U. S. Army Engineer Waterways Experiment Station, Weapons Effects Laboratory, P. O. Box 631, Vicksburg, Miss. 39180
10. PROGRAM ELEMENT, PROJECT, TASK AREA & WORK UNIT NUMBERS: Project No. 4A061101A91D
11. CONTROLLING OFFICE NAME AND ADDRESS: Office, Chief of Engineers, U. S. Army, Washington, D. C. 20314
12. REPORT DATE: June 1976
13. NUMBER OF PAGES: 70
14. MONITORING AGENCY NAME & ADDRESS (if different from Controlling Office): 74p.
15. SECURITY CLASS. (of this report): Unclassified
15a. DECLASSIFICATION/DOWNGRADING SCHEDULE
16. DISTRIBUTION STATEMENT (of this Report): Approved for public release; distribution unlimited.
14. WES-MP-N-76-10
17. DISTRIBUTION STATEMENT (of the abstract entered in Block 20, if different from Report)
16. DA-H-A-061101-A-91-D
18. SUPPLEMENTARY NOTES
19. KEY WORDS (Continue on reverse side if necessary and identify by block number)

Explosion effects
Ground motion predictions
Ground shock
Impact
Sandstones

20. ABSTRACT (Continue on reverse side if necessary and identify by block number)

A technique for prediction of ground motions in the transition and far-out regions where outrunning surface waves are transporting most of the energy is described.

A statistically significant number of surface ground motion velocity measurements were produced by detonating high-explosive (HE) spheres of differing yields and depths of burst. Similar measurements were obtained from energy sources realized by impacting free-falling weights.

The tests in this study were conducted on a nearly homogeneous sandstone formation in October 1973 at a

(Continued) → next pg

DD FORM 1 JAN 73 1473 EDITION OF 1 NOV 65 IS OBSOLETE

Unclassified

SECURITY CLASSIFICATION OF THIS PAGE (When Data Entered)

038 100 LB

Destroy this report when no longer needed. Do not return it to the originator.

20. ABSTRACT (Continued).

site near Grand Junction, Colorado, along with Project CENSE (Coupling Efficiency of Near Surface Explosions). The CENSE series consisted of detonations of eight 1000-lb nitromethane spheres and the SHE (Small High Explosive) series consisted of 20 detonations of C-4 spheres ranging in weights from 1 to 27 lb. Fourteen SMIT (Spherical Mass Impact Technique) tests were conducted by releasing a 6800-lb demolition ball from heights ranging from 20 to 40 ft.

Dimensional analysis produced a scaling method in which vertical velocity at any given range scales by charge weight to the one-sixth power ($W^{1/6}$). This scaling is borne out by data from large-scale HE and nuclear tests, from which independent linear regression produced essentially the same scaling. All wave forms, both explosive and impact created, exhibit the same characteristic similarities. HE prediction equations were developed from correlations between the impact and surface tangent ground motion data, using the impact results as the model and the explosive results as the prototype. Because the vertical ground motion data were relatively insensitive to depth of burst, the prediction equations should be relatively accurate for depths of burst in the range of plus or minus one charge radius.

THE CONTENTS OF THIS REPORT ARE NOT TO BE USED FOR ADVERTISING, PUBLICATION, OR PROMOTIONAL PURPOSES. CITATION OF TRADE NAMES DOES NOT CONSTITUTE AN OFFICIAL ENDORSEMENT OR APPROVAL OF THE USE OF SUCH COMMERCIAL PRODUCTS.

PREFACE

This investigation was conducted by personnel of the U. S. Army Engineer Waterways Experiment Station (WES) and sponsored by the Office, Chief of Engineers, Department of the Army, under Project No. 4A061101A91D, In-House Laboratory Independent Research Program. These experiments were conducted in the study of explosion produced Rayleigh wave prediction by means of a nonexplosive source.

The field investigations were performed in October 1973 under the direction of Mr. J. G. Wallace, Project Engineer. The data analysis was accomplished by Messrs. Wallace, M. B. Ford, and J. L. Drake. This report was prepared by Mr. Ford. The work was accomplished under the general supervision of Mr. W. J. Flathau, Chief of the Weapons Effects Laboratory, and under the direct supervision of Mr. L. F. Ingram, Chief of the Phenomenology and Effects Division.

COL G. H. Hilt, CE, and COL J. L. Cannon, CE, were Directors of WES during the investigation and publication of this report; Mr. F. R. Brown was Technical Director.

CONTENTS

CONVERSION FACTORS, U. S. CUSTOMARY TO METRIC (SI) UNITS OF MEASUREMENT

U. S. customary units of measurement used in this report can be converted to metric (SI) units as follows:

Multiply	By	To Obtain
inches	0.0254	metres
feet	0.3048	metres
miles (U. S. statute)	1.609344	kilometres
cubic feet	0.02831685	cubic metres
pounds (mass)	0.4535924	kilograms
tons (short)	907.1847	kilograms
inches per second	0.0254	metres per second
feet per second	0.3048	metres per second
foot-pounds (force)	1.355818	newton-metres

CORRELATION OF IMPACT AND EXPLOSIVELY CREATED GROUND SHOCK PHENOMENA

PART I: INTRODUCTION

BACKGROUND

1. Extensive research effort has been devoted to the development of a better understanding of ground motions associated with explosively produced craters. Although much of this effort was stimulated by the need to design underground structures capable of resisting nuclear weapon effects, the resulting information is also useful in analysis and design against earthquakes, excavation with explosives, and other sources of vibrations which affect structures adversely.

2. In spite of the numerous explosion effects studies conducted to date there still exist many uncertainties in several ground motion regimes of interest which need to be investigated. The military has been primarily concerned with strong ground shock close to the energy source; others have been interested in long-range detection of earthquakes and arrival times which are useful in geophysical investigations.

3. As energy is propagated from a cratering explosive source it is characterized by various modes of propagation and dissipation with range from the source. Direct coupling and airblast effects dominate the motions near the explosion. These early-time close-in motions are reasonably well understood and are characterized by high amplitude and high frequency P-waves and S-waves. As the range from the source increases the modes of wave propagation evolve such that the majority of the energy is transported by surface waves characterized by relatively large amplitudes and low frequencies. The physics of this evolution with range is poorly understood. The close-in motions are strongly influenced by parameters such as the explosive, yield, geometry, depth of burst, geology, and material properties. The motions at later times, however, seem to be less sensitive to some of these parameters. A recent study (Reference 1) indicated that a well-defined energy source (falling weights) could be used to isolate the directly induced motions from any airblast effects. Favorable conclusions were made concerning the possibility of correlating mechanical impact and explosively created surface motions in the far-out regions.

PURPOSE AND SCOPE

4. Reliable predictions of ground motions (particularly peak particle velocity and wave frequency content) are needed to determine the feasibility of all explosive projects. In many cases the most critical motions occur in the transition and far-out regions where outrunning surface waves are transporting most of the energy.

5. The specific objectives of this study were to (a) obtain a statistically significant number of surface ground motion velocity measurements in the transition and far-out regions produced by detonating high-explosive (HE) spheres of differing yields and depths of burst, (b) record similar measurements for energy sources caused by the impact of free-falling weights, (c) reduce the data in a

form such that it could be analyzed with the aid of dimensional analysis to develop correlations between the HE and impact ground motion phenomena, and (d) develop HE prediction equations from the correlations using the impact results as the model and the explosive results as the prototype.

6. The tests were conducted on a nearly homogeneous sandstone formation in October 1973 at a site near Grand Junction, Colorado (Figure 1). The test site selection was based on the opportunity to participate in Project CENSE (Coupling Efficiency of Near Surface Explosions) which increased the scope of the planned HE yields by a factor of about 30 in terms of explosive weights. The CENSE series consisted of the detonation of eight 1000-lb* nitromethane spheres (Reference 2), and the SHE (Small High Explosive) series consisted of 20 detonations of C-4 spheres ranging in weights from 1 to 27 lb. Fourteen SMIT (Spherical Mass Impact Technique) tests were conducted by releasing a 6800-lb demolition ball from heights ranging from 20 to 40 ft. Additional data are available from the Mixed Company event (Reference 3) which was a 500-ton TNT detonation over this sandstone formation.

7. This report describes the tests conducted, instrumentation used, data reduction methods, and empirical relations established, and discusses the results. All the data are stored on magnetic tape for future use if needed.

---

* A table of factors for converting U. S. customary units of measurement to metric (SI) units is presented on page 4.

PART II: PROCEDURE

TEST SITE DESCRIPTION

8. A detailed topographic map of the Grand Junction test site area is shown in Figure 2. The overburden was removed from the hatched area on the map with a motor patrol grader to expose the underlying rock. A previous geophysical investigation (Reference 3) identified the exposed rock as a part of the Kayenta sandstone formation in the Glen Canyon Group. The stratum is approximately 70 ft thick and overlies a Wingate sandstone formation approximately 300 ft thick. A large protrusion of exposed Entrada sandstone lies north of the test site.

9. Although borings to 85 ft did not reveal any major horizontal faults, there were visible surface joints of undetermined depth randomly scattered over the test area.

EXPERIMENTAL PLAN

10. Locations for 10 instrument stations spaced at 50-ft intervals were selected for use in all the tests conducted at this site. The instrument plan is shown in Figure 3. The locations of the CENSE 1000-lb nitromethane detonations are also shown in Figure 3. The depth of burst configurations for the explosive charges are shown in Figure 4. The locations of the SHE detonations and the impact tests are not shown, but the instrument stations defined a reasonably good radial line from ground zero for all of the tests conducted. Twenty-eight HE tests and 14 impact tests were conducted. Twelve channels of ground motion measurements were recorded in analog form on magnetic tapes during each test.

11. Ten vertical and two horizontal surface ground motion measurements were made during each test. The horizontal measurements were made in a radial direction to ground zero. Two types of velocity gages were used during the tests. The velocity gages used for the 1000-lb nitromethane detonations were MB Corporation Model 120 (natural frequency, 2.5 Hz; damping, 65 percent; sensitivity, 38 mv/cm/sec), and the velocity gages used in all other tests were the more sensitive GEO SPACE Model HS-10-1 (natural frequency, 1 Hz; damping, 70 percent; sensitivity, 3 v/cm/sec). The two stations nearest ground zero in the CENSE tests and the first station in the SHE and SMIT tests were instrumented with vertical sensing Kistler Instrument Corporation Model 303B servo-accelerometers (natural frequency, 300 Hz; adjustable sensitivity, 10 - 0.1 v/g). The radially oriented horizontal velocity gages were located at the stations shown in Figure 3. The gages were interfaced with compatible signal conditioning equipment and calibration panels driving an FM magnetic tape recorder operating at 7-1/2 in./sec. All electronic recording equipment was housed in the WES recording van approximately 2000 ft from the ground zero area.

12. The MB Corporation velocity gages were placed by epoxying a small aluminum mounting block to competent sandstone at each station and then the gages were firmly bolted to the block. This facilitated removal of the gages during inclement weather. The HS-10-1 velocity gages were placed in shallow boreholes and firmly grouted to the sandstone with neat gypsum cement grout. Sandbags were also placed over the gages to increase the mass restraining the gages. The servo-accelerometers were mounted in small aluminum canisters filled with paraffin for protection. The canisters were grouted into shallow boreholes in the sandstone with neat gypsum cement grout. All electrical signals were carried to the recording van with Belden four-wire shielded cable.

13. Approximately 30 min prior to zero time, all gages were electrically calibrated on tape with a

step function proportional to a known velocity or acceleration. This procedure was repeated after each test to verify the calibration and record any possible electrical drift. The magnetic tape was played back on an oscillograph to confirm that acceptable data were obtained and to assure that a permanent record was made in the event the magnetic tape was accidently erased before it could be processed.

DESCRIPTION OF EXPLOSIVE TESTS

14. The experimental geometry of the explosive tests conducted is shown in Figure 5. A tabulation of the horizontal range from ground zero to the first instrument station is given in Appendix A for each event. The ranges to the other instrument stations are determined by progressively adding 50 ft to the range from the previous station.

15. The 1000-lb charges were formed by pouring liquid nitromethane into 3-ft-diam hollow fiberglass spheres manufactured by the Physics International Company as shown in Figure 6. Central detonation of the nitromethane spheres was accomplished with a Reynolds Industry RP-1M exploding bridge wire in approximately 0.5 lb of C-4 booster. The exploding bridge wire was used as the initiating detonator for safety reasons, since some of the nitromethane charges had to be loaded several days prior to detonation. A block diagram of the firing circuit is shown in Figure 7. Extreme caution should be observed when this method of detonation is used under irreversible conditions such as an inaccessible buried charge. The firing supply must provide enough energy to explode the wire which detonates the secondary booster. In this case it was necessary to locate the 2500-v d-c firing supply only 300 ft from ground zero to achieve detonation. Attempts to explode the wire with the supply located in the recording van simply burned the wire. Fortunately, this occurred on the elevated charge and it was possible to replace the booster package.

16. The SHE spherical charges were manually shaped from 1.25-lb blocks of C-4 composition explosive. The charge density was controlled by packing the spheres to within ±5 percent of the original blocks. The charges were centrally detonated with U. S. Corps of Engineers special electric blasting caps.

DESCRIPTION OF THE IMPACT TESTS

17. The impact tests were accomplished with a 6800-lb iron demolition ball and a 45-ton crane with a 105-ft boom. The weight was attached to the boom with a 5-ft loop of 3/8-in. steel cable. The crane was capable of raising the weight to a maximum height of 40 ft in this configuration. The weight was released for free fall by cutting the 3/8-in. cable with 25-grain Primacord. An effective method of cutting the cable was found to be four layers of tightly wound loops of Primacord. The first layer had 12 loops, the second layer had 10 loops, the third layer had 8 loops, and the fourth layer had 6 loops of 25-grain Primacord. A typical test is shown in Figure 8. A total of 14 tests was conducted. The drop heights ranged from 20 to 40 ft and the radial range to the first instrument station varied from 25 to 60 ft. It was observed that the weight rebounded approximately 5 to 10 ft after impact.

PART III: RESULTS

DATA REDUCTION

18. The analog tapes were digitized on a high-speed digital converter and recorded on magnetic tape in card-image binary-coded decimal form for input to Fortran data processing codes. The digital tapes were processed through a Honeywell G-635 computer and standard Waterways Experiment Station (WES) codes were applied to extract correlatable quantities from the data. These routines included integration, plot tapes, and fast Fourier transforms. The velocity-time histories and fast Fourier transforms were automatically plotted from the plot tapes on an off-line plotter. Some typical vertical velocity-time histories are presented in Figures 9-11. All time scales are the same, but the velocity scales are arbitrary. All of the velocity records were manually analyzed to obtain maximum peak-to-peak amplitudes, associated periods and group wave speed of the "ground roll," or Rayleigh wave-type motion, exclusive of airblast. The values for each test were tabulated and stored in a data bank which included energy at source, range to ground zero, crater dimensions, peak acceleration, and duration t_d* of the demolition ball in the impact tests.

19. Similitude theory (dimensional analysis) was determined to be the best approach to the data analysis. This method of attack allows normalization of the data to facilitate development of meaningful relationships between the explosive and the impact phenomena.

20. The initial step in any investigation utilizing dimensional analysis is the accurate determination of the variables which influence the phenomenon. It is then possible to express each variable in terms of its basic dimensions such as, in this particular case, force F, length L, and time T. The Buckingham Pi theorem maintains that any complete physical relationship can be described by a set of dimensionless products (pi terms) composed of relevant physical parameters (Reference 4). The number of pi terms necessary to describe a phenomenon is the original number of variables, n, less the number of basic dimensions, s.

21. The significant parameters assumed to be associated with the outrunning ground surface motion for this study are tabulated below:

Quantity	Basic Dimensions
E = total energy at source	FL
D = depth of charge burial, center	L
r_c = effective charge radius	L
g = acceleration due to gravity	LT^{-2}
γ = mass density of the soil	FL^{-3}
d_a = crater depth	L
r_a = crater radius	L
R = ground range from source	L
V = peak-to-peak particle velocity of Rayleigh wave at range, R	LT^{-1}
T = Rayleigh wave period	T
V_s = Rayleigh wave speed (group velocity)	LT^{-1}
a_p = peak deceleration of weight during impact	LT^{-2}
t_d = duration of deceleration pulse	T

* For convenience, symbols and unusual abbreviations are listed and defined in the Notation (Appendix D).

Pi terms found to influence the ground roll phenomenon significantly are:

$$\frac{E}{\gamma R^4}, \frac{a_p t_d}{2gh}, \frac{R}{r_c}, \frac{VT}{R}, \frac{V^2}{gR}, \frac{V}{V_s}$$

The first two terms can be interpreted as normalized potential energy and normalized peak velocity of the spheres during impact, respectively. They apply only to the comparison between the SMIT sandstone tests and the WES tests previously performed at Vicksburg (Reference 1). The remaining normalized seismic parameters can be physically interpreted as: (a) R/r_c is a scaled range from the seismic source, (b) VT/R is a normalized particle displacement, (c) V^2/gR is a normalized particle kinetic energy, and (d) V/V_s is a normalized particle velocity.

22. The effective charge radius r_c was calculated for explosive and impact tests from the total available energy, using TNT as the standard, thus providing a unifying energy link to all tests, regardless of energy source.

23. The explosive tests consisted of the series of 1000-lb nitromethane (CENSE) tests and the 20 SHE tests with charges ranging from 1 to 27 lb of C-4. Although good data were obtained from the CENSE tests, many of the SHE tests produced relatively poor wave forms which bordered on the noise band. Also, the effect of the thin weather-fractured surface rock layer to attenuate the ground roll was exaggerated by the low yields.

24. The compressional wave arrival times for the explosive tests indicated an average velocity of approximately 9000 ft/sec. The dominant wave group (ground roll) velocity averaged 3300 ft/sec, which is very close to the 3510 ft/sec observed for the 500-ton Mixed Company event conducted on the same rock formation several miles away (Reference 3). A comparison of typical explosive-induced vertical and radial velocity-time histories and the associated Rayleigh wave particle motions is shown in Figure 12.

25. The peak-to-peak particle velocity amplitude V, period of motion T, and Rayleigh wave group velocity V_s are used to characterize the ground motion. The above seismic descriptors are identified in Figure 13. The other variables associated with the experiment were energy level, characterized by effective charge radius r_c, and range R from the seismic source.

26. Only the surface-tangent shots are presented here because they are more easily relatable to the impact tests, and because they allow the inclusion of the 500-ton Mixed Company data. Plots of the data at all depths of burial (DOB) are included in Appendix B.

VERTICAL EXPLOSIVE RESULTS

27. Plots of the best correlations are shown in Figures 14 and 15. Applying a least-squares fit to the data yields the following equations:

$$\frac{V^2}{gR} = 950 \left(\frac{R}{r_c}\right)^{-3.92} \quad (1)$$

$$\frac{VT}{R} = 0.989 \left(\frac{R}{r_c}\right)^{-2.155} \quad (2)$$

28. The plot in Figure 16, V/V_s versus R/r_c, has the general equation

$$\frac{V}{V_s} = C_1 \left(\frac{R}{W^{1/3}}\right)^{-n} \quad (3)$$

since $r_c^3 \propto W$.

By its nature, this plot implies that range scales by $W^{1/3}$ and that velocity scales with V_s but is unscaled by yield. The plot appears to be at least two separate parallel data bands with the spread ordered by W. Apparently scaling the range by $W^{1/3}$ does not hold for the spread of charge weights tested. The additional scaling necessary to bring the data together is provided in Figure 14. The general form of the least-squares fit (Equation 1) may be written as:

$$\frac{V^2}{gR} = C_2 \left(\frac{R}{W^{1/3}}\right)^{-n} \quad (4)$$

Isolating the scaled range $R/W^{1/3}$ to the right side of the equation and taking the square root of both sides results in Equation 5.

$$\frac{V}{W^{1/6}} = (C_2 g)^{1/2} \left(\frac{R}{W^{1/3}}\right)^{(1-n)/2} \quad (5)$$

This indicates that $V \propto W^{1/6}$.

29. Figure 15 shows normalized particle displacement plotted against scaled range. Again substituting $W^{1/3}$ for r_c and generalizing Equation 2 yields

$$\frac{VT}{R} = C_3 \left(\frac{R}{W^{1/3}}\right)^{-m} \quad (6)$$

Isolating the scaled range to one side results in the following equation:

$$\frac{VT}{W^{1/3}} = C_3 \left(\frac{R}{W^{1/3}}\right)^{1-m} \quad (7)$$

Since it was again assumed that $R \propto W^{1/3}$, VT must be proportional to $W^{1/3}$. It follows that

$$\frac{V}{W^{n_1}} \times \frac{T}{W^{n_2}} = \frac{VT}{W^{1/3}} \quad (8)$$

where

$$n_1 + n_2 = \frac{1}{3}$$

The values for n_1 and n_2 must now be determined. From Equation 5 it is evident that $V \propto W^{1/6}$. Substituting this value into Equation 8 as n_1 indicates that n_2 must also be 1/6. Therefore $V \propto W^{1/6}$ and $T \propto W^{1/6}$. Further evidence that the period T scales by $W^{1/6}$ is obtained by examining the periods and frequency spectra of the velocity-time histories.

30. Figure 17 compares the composite frequency spectra of the Mixed Company, CENSE, and SHE 4-lb tests. Taking the reciprocal of the frequency at the peak amplitude of each test gives the average period for each test. Figure 18 shows the period T plotted against scaled range. An eyeball fit of each set of test data was chosen such that the fits were parallel for all tests. The intercepts at a scaled range of 100 were plotted in Figure 19, along with the periods determined from Figure 18. A line with a slope of 1/6 is drawn through the points, indicating that if the Mixed Company data are included, $W^{1/6}$ scaling of T provides a reasonable fit for the data.

RADIAL EXPLOSIVE RESULTS

31. The two radial measurements for each test of the CENSE and SHE series were made at stations 6 and 10 (Figure 3). Plots using the same parameters as utilized in the analysis of the vertical data are shown in Figures 20-22. All three plots appear to contain about the same amount of scatter. The two points of the CENSE and of each of the SHE tests form a series of stacked parallel lines with different slopes than the Mixed Company data. The amount of data is insufficient to form any definite conclusion as to how good the correlation is for these plots.

32. Figure 23 shows a plot of the period T versus scaled range. The intercepts of the parallel line fits, taken at a scaled range of 1,000, are plotted as a function of charge weight in Figure 24. This figure indicates that T scales by $W^{1/6}$ for $1 \leq W \leq 1{,}000$, but that scaling by $W^{1/3}$ provides a better fit between W = 1,000 and W = 1,000,000 lb. Equations derived from Figures 20-22 are:

$$\frac{V^2}{gR} = 3.39 \left(\frac{R}{r_c}\right)^{-3.05} \tag{9}$$

$$\frac{VT}{R} = 0.13 \left(\frac{R}{r_c}\right)^{-1.83} \tag{10}$$

$$\frac{V}{V_s} = 0.50 \left(\frac{R}{r_c}\right)^{-1.80} \tag{11}$$

33. All explosive tests, except for the CENSE shot buried at seven charge radii, appeared relatively insensitive to DOB. This included DOB's in a range from four charge radii above (airburst) to one charge radius below (fully buried). The fact that Froude scaling tightens the vertical data suggests that gravity is a significant factor in ground roll, tending to pull the ground surface back down as it is lifted upward. The radial data were insufficient to determine DOB effect.

34. Scaling by crater parameters and other pertinent quantities failed to bring the data together as tight as the plots shown.

IMPACT RESULTS

35. The impact data were obtained by dropping a 6800-lb iron demolition ball from heights of 20 and 40 ft. The first drop was from 20 ft and the remaining 13 drops were from 40 ft. The potential energy E of the seismic source was used for all calculations. Typical vertical and radial velocity-time histories are compared and the associated particle motion path presented in Figure 25.

36. The data are plotted with the same parameters that were applied to the explosive data. These plots, Figures 26-28, appear reasonably tight. The 20-ft drop scales well with the 40-ft drop. Lack of variation in the tests, however, necessitates reliance upon the tests conducted in soil at WES (Reference 1) to conclude that these parameters scale the impact-produced Rayleigh waves propagated through sandstone. The vertical wave period is plotted as a function of scaled range in Figure 29. The comparison of craters produced by different drop heights could not be made as in soil. Crater dimensions of both the impact and explosive tests are presented in Appendix C. The radial motion data are not discussed because the amount was inadequate to extract any reliable information; however, the data points are included for completeness in Figures 30-32.

37. Equations for the plots in Figures 26-28 are:

$$\frac{V^2}{gR} = 2.054 \times 10^6 \left(\frac{R}{r_c}\right)^{-4.05} \tag{12}$$

$$\frac{VT}{R} = 80.0 \left(\frac{R}{r_c}\right)^{-2.26} \tag{13}$$

$$\frac{V}{V_s} = 1.84 \left(\frac{R}{r_c}\right)^{-1.63} \tag{14}$$

As in the explosive data, the plots with V and T both scaled by $W^{1/6}$ give the best fits (Figures 26 and 27). Also T increases more rapidly with R/r_c than in the explosive tests. The wave forms in Figure 25 closely resemble those shown in Figure 12 (explosive), indicating that the source is similar. Energy equivalence and correlations will be discussed in the next section.

PART IV: CORRELATIONS BETWEEN HIGH EXPLOSIVE AND IMPACT DATA

INTRODUCTION

38. Results of the explosive and impact tests affirm that the SMIT can be used to determine certain characteristic properties of a particular geological site. Based on these results, equations were developed to predict Rayleigh motions for the CENSE-SMIT test site in Colorado. These equations should be adaptable to other sites by inclusion of a media property distortion function.

39. The vertical spectra plot in Figure 33 shows that the SMIT Rayleigh wave frequency is in the same range as the SHE wave frequency, with the SMIT spectra being somewhat tighter, indicating the absence of airblast effects and other extraneous signals produced by explosives. In this respect it is very similar to the large-scale Mixed Company spectra shown in Figure 17. This should make the SMIT very useful in the study of outrunning motions produced by small yields in which the signal is often intermingled with airblast effects and extraneous noise. Figure 34 compares the vertical velocity-time histories of the various explosive tests with the impact wave form. The wave form is compressed time-wise as the charge weight decreases, but this compression is pronounced only between the Mixed Company and the CENSE wave forms. Because T is proportional to $W^{1/6}$ there is very little compressional difference between the CENSE, SHE, and SMIT wave forms. The relationships of the initial peak amplitudes vary from test to test, but it is especially important to note that all of the wave forms are basically similar.

40. The explosives and impact vertical data are compared in Figures 35-37. Because the slopes of vertical explosive and impact plots are almost identical (Equations 1, 4, 12, and 13), forcing the lines described by the corresponding equations to be parallel will not have any noticeable effect on the data and will simplify calculations. The new equations are:

$$\frac{V_e^2}{gR} = 2357 \left(\frac{R}{r_c}\right)^{-4} \tag{15}$$

$$\frac{V_i^2}{gR} = 1.073 \times 10^6 \left(\frac{R}{r_c}\right)^{-4} \tag{16}$$

$$\frac{V_e T_e}{R} = 1.428 \left(\frac{R}{r_c}\right)^{-2.2} \tag{17}$$

$$\frac{V_i T_i}{R} = 54.76 \left(\frac{R}{r_c}\right)^{-2.2} \tag{18}$$

Comparison of the explosive and the impact data was approached in two ways:

a. Effectiveness concept – ratio of the effect produced by explosive and by impact at the same scaled range.

b. Equivalent effect concept—the percent of impact energy required to produce the same effect (V^2/gR or VT/R) by explosive means.

EFFECTIVENESS CONCEPT

41. The plot V^2/gR versus R/r_c in Figure 35 is analyzed to determine the ratio of explosion-produced peak-to-peak particle velocity to the impact-produced velocity at the same range with the same potential energy (effective charge radius). Dividing Equation 15 by Equation 16 gives

$$\frac{V_e^2}{gR} = 1.38 \times 10^{-3} \frac{V_i^2}{gR} \tag{19}$$

Dividing out gR on both sides and taking the square root gives the equation:

$$V_e \simeq \frac{1}{27} V_i \tag{20}$$

This indicates that the vertical particle velocity produced by an explosion would be 1/27th the velocity produced by an impact, with the same range and equivalent energy.

42. Similarly, considering the plot of VT/R versus R/r_c shown in Figure 36, divide Equation 17 by Equation 18 to obtain

$$V_e T_e = \frac{1}{38} V_i T_i \tag{21}$$

The spherical mass impact-induced displacement is 38 times greater than that produced by an explosion of equivalent potential energy at the same range. Going a step further, substitute Equation 20 into Equation 21 and solve for T_e to get

$$T_e = 0.71 \, T_i \tag{22}$$

This implies that for the same range and energy, the impact-produced period is 1.4 times longer than the explosion-related period.

EQUIVALENT EFFECT CONCEPT

43. Examine the V^2/gR versus R/r_c plot from the equivalent effect viewpoint, the explosive to impact yield ratio $(r_c)_e/(r_c)_i$ that will produce the same effect (V^2/gR) at the same range. Set Equation 15 equal to Equation 16 and take the fourth root of both sides to get

$$\frac{R_e}{(r_c)_e} = 0.193 \frac{R_i}{(r_c)_i} \tag{23}$$

Since $R_e = R_i$, divide out R and rearrange the terms to get

$$(r_c)_e = 5.2\ (r_c)_i$$

but

$$r_c^3 \propto E$$

so that

$$\frac{E_e}{E_i} = (5.2)^3$$

or

$$E_e = 139\ E_i \tag{24}$$

Therefore, the explosive energy must be 139 times greater than the impact energy to produce the same effect at the same range. Applying the same concept to the nondimensional displacement plot in Figure 36, start with:

$$\frac{V_e T_e}{R_e} = \frac{V_i T_i}{R_i} \tag{25}$$

where

$$R_e = R_i$$

by nature of the equivalent effect concept. Set Equation 17 equal to Equation 20 and simplify to obtain

$$(r_c)_e = 5.24\ (r_c)_i \tag{26}$$

which must be cubed to relate to potential energy, so

$$E_e = 144\ E_i \tag{27}$$

Equation 27 agrees with Equation 24 which was derived from the nondimensional kinetic energy plot in Figure 35.

RADIAL DATA

44. Plots of the radial SMIT and explosive data are shown in Figures 30-32. No attempt was made at comparison because the data were insufficient to draw a sound conclusion.

PART V: COMPARISON OF SPHERICAL MASS IMPACT TECHNIQUE IN ROCK AND SOIL

45. Because there was essentially no variation in potential energy in the Colorado SMIT test series, it is difficult to relate to the earlier test conducted in soil at WES. An attempt was made here, however, to compare certain parameters developed in the report (Reference 1) by Wallace and Fowler. A characteristic nondimensional force-time function $F(\tau)$ was developed which is constant, regardless of energy level or sphere geometry, for a particular test site and the SMIT method of creating a seismic source. This function is described by the equation

$$\frac{\sqrt{2gh}}{a_p t_d} = \int_0^1 F(\tau)d\tau \tag{28}$$

where

a_p = peak deceleration of the sphere during impact
t_d = time of duration of deceleration pulse
$\sqrt{2gh}$ = impact velocity of sphere

A plot of the potential energy of the seismic source versus the dimensionless parameter defined in Equation 24 indicates that statistically (Figure 38)

$$\frac{a_p t_d}{\sqrt{2gh}} = 1.85 \tag{29}$$

for the WES test site and

$$\frac{a_p t_d}{\sqrt{2gh}} = 2.75 \tag{30}$$

for the Colorado SMIT test site. This number is the ratio of the area under the deceleration curve (equal to impact velocity of the sphere) to the area of a rectangle with height a_p and width t_d. Tabulated below are values for different types of curves.

Type Curve	$\frac{a_p t_d}{\sqrt{2gh}}$
Rectangular	1
Triangular	2
Sinusoidal	1.54

Figure 39 illustrates the reason for the number in Equation 30 being greater than 2.

46. The Colorado SMIT data were plotted for comparison with the data from the WES drops in soil (Figures 40 and 41). The kinetic energy plot in Figure 40 appears to bring the two sets of data

together for these particular energy levels, but how this can be related to the explosive tests is not apparent. Figure 41 indicates that the data bands of the sandstone and the soil test are not parallel; therefore, a media distortion factor is necessary to bring the data from two geologically different sites together. A more detailed and informative analysis would require further tests specifically designed for this comparison.

PART VI: DISCUSSION AND CONCLUSIONS

47. Good correlations were developed between the impact and the surface-tangent explosive ground motion data. Specific conclusions extrapolated from the impact and surface-tangent HE vertical ground motion data are:

a. At a given range and energy level, the impact-produced peak particle velocity is 27 times greater than that produced by an explosion; the impact-produced displacement is 38 times greater than that produced by an explosion; the period of impact-produced ground motion is 1.4 times longer than the period of explosion-produced ground motion.

b. The potential explosive energy must be approximately 140 times greater than the impact energy to produce the same effect at the same range. This can be attributed to the fact that much of the explosive energy for near-surface shots is expended into the atmosphere as airblast, into crater formation, and dissipated as heat, whereas essentially all of the impact energy is available to produce ground motion.

c. At a given range the particle velocity scales by the charge weight to the one-sixth power ($W^{1/6}$); the period of motion also scales by the charge weight to the one-sixth power.

d. The explosive wave forms tended to exhibit the same general characteristics, from the 1-lb SHE tests through the 500-ton Mixed Company test. The impact wave forms showed the same characteristics, having slightly greater velocities and periods than the SHE wave forms, probably due to the gage placement being closer to the seismic source. The wave forms were much cleaner than those of SHE and CENSE, more closely resembling the 500-ton Mixed Company wave forms in this respect.

48. Radial motion results were inconclusive due to the limited amount of data available. It was observed, however, that the surface-tangent explosion-produced periods of motion scale with charge weight to the one-sixth power ($W^{1/6}$) for $1 \leq W \leq 1{,}000$, but scale with charge weight to the one-third power ($W^{1/3}$) for $1{,}000 \leq W \leq 1{,}000{,}000$ (CENSE and Mixed Company).

49. A statistically significant number of vertical velocity measurements of surface ground motion in the transition and far-out regions were produced by detonating HE spheres of different yields and depths of burst. It was anticipated that similar measurements would be recorded for energy sources caused by the impact of free-falling weights dropped from various heights. The use of the impact technique in rock, however, was unfamiliar. In an attempt to produce impact craters in the sandstone for comparison with HE-formed craters and to obtain a signal adequate to register on the instrumentation, all drops but one were released from a maximum obtainable height of 40 ft. Because only one drop height was used, it was impossible to see if the impact data scaled by the parameters used for the explosive data. Comparison of craters created by drops from different heights was also not possible. Only two radial velocity measurements were made for each test, both explosive and impact, as compared to 10 measurements for the vertical ground motion data. It was realized during the data analysis that more extensive radial instrumentation would have allowed more definite conclusions concerning the far-out radial ground motion.

50. The dimensional analysis yielded a scaling method which implies that gravity influences vertical ground motion. For any given range vertical velocity scales with charge weight to the one-sixth power ($W^{1/6}$). This scaling is borne out by data from large-scale nuclear tests in Reference 5 by W. V. Mickey and data from charges ranging from 1 ton to approximately 43 tons in Reference 6 by

Thomas M. Tami. Although equations in these reports were derived by independent linear regression, they arrive at essentially the same result as the approach used in this report (which was determined by the dimensional analysis). Manipulation of the Mickey and Tami equations shows that the vertical velocity is proportional to charge weight to approximately the one-sixth power. Particularly interesting is the fact that this relation holds over such a broad range of charge yields.

51. Correlations developed in this report should also hold for near-surface explosions within the DOB range of plus or minus one charge radius, since inclusion of the various near-surface DOB data merely increased the scatter of the trend established by the surface-tangent data rather than indicating any trend with increasing DOB. This insensitivity to DOB was also observed in the close-in CENSE vertical data (Reference 2). Additional testing of both explosives and the SMIT in various media should enable the impact technique to yield relatively accurate predictions of explosive peak particle velocity, period of motion, and wave speed at unknown test sites.

REFERENCES

1. Wallace, J. G. and Fowler, J., "Fundamental Experiments in Ground Shock Phenomenology," Miscellaneous Paper N-73-2, Mar 1973, U. S. Army Engineer Waterways Experiment Station, CE, Vicksburg, Miss.
2. Ingram, J. K., Drake, J. L., and Ingram, L. F., "Influence of Burst Position on Airblast, Ground Shock, and Cratering in Sandstone," Miscellaneous Paper N-75-3, May 1975, U. S. Army Engineer Waterways Experiment Station, CE, Vicksburg, Miss.
3. Ingram, J. K., "Middle North Series Mixed Company Event - Ground Shock from a 500-Ton High-Explosive Detonation on Soil Over Sandstone," POR 6613, Aug 1975, U. S. Army Engineer Waterways Experiment Station, CE, Vicksburg, Miss.
4. Murphy, G., *Similitude in Engineering*, Ronald Press, New York, 1950.
5. Mickey, W. V., "Seismic Wave Propagation," *Third Plowshare Symposium*, 21-23 Apr 1964, University of California.
6. Tami, T. M., "Analysis of Ground-Motion Peak Particle Velocities from Cratering Experiments at Trinidad, Colorado," Miscellaneous Paper E-73-3, May 1973, U. S. Army Engineer Waterways Experiment Station, CE, Vicksburg, Miss.

Figure 1. Projects CENSE and SMIT test site general location map

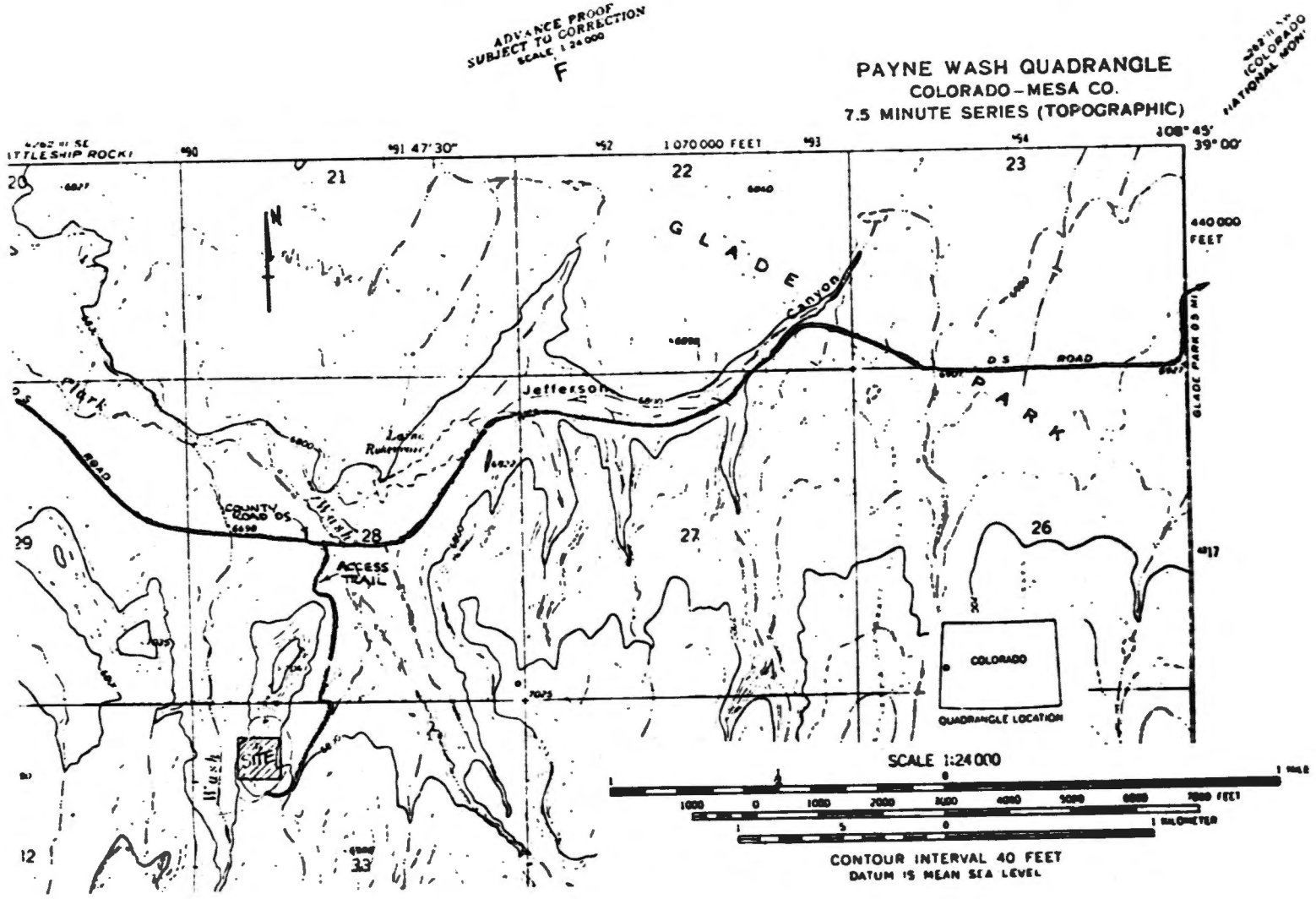

Figure 2. Projects CENSE and SMIT test site detail topographic map

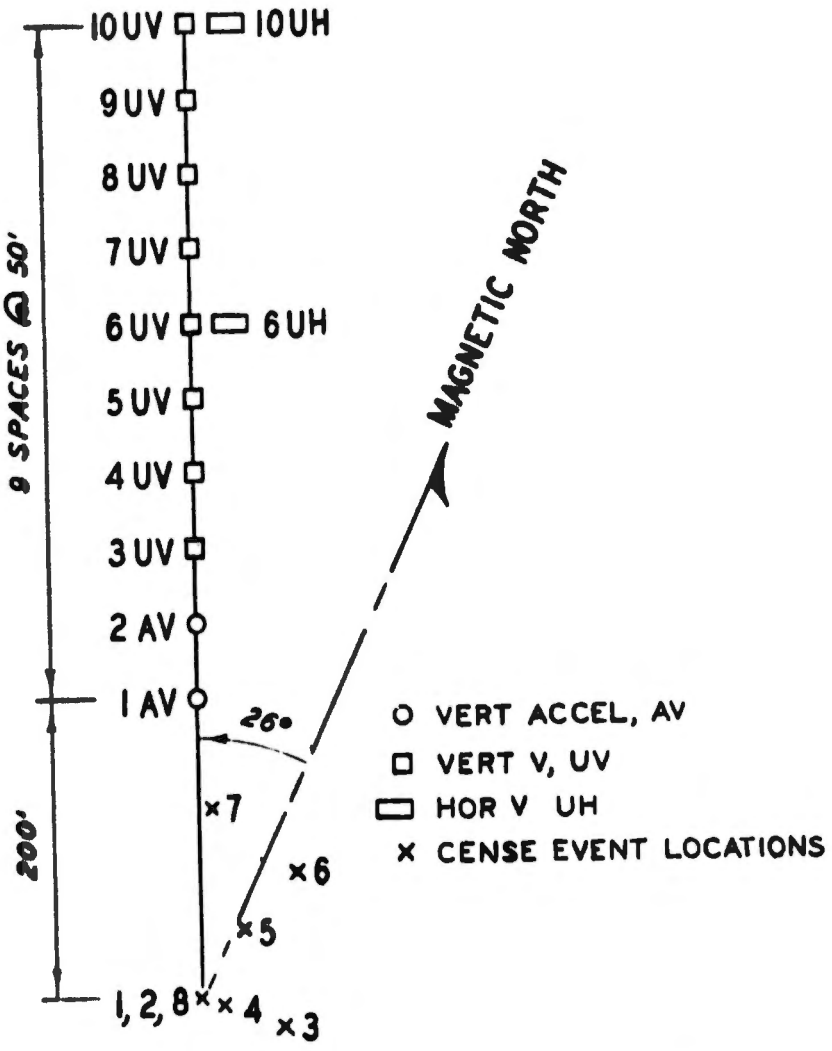

Figure 3. Plan view of the instrument array and location of the CENSE events

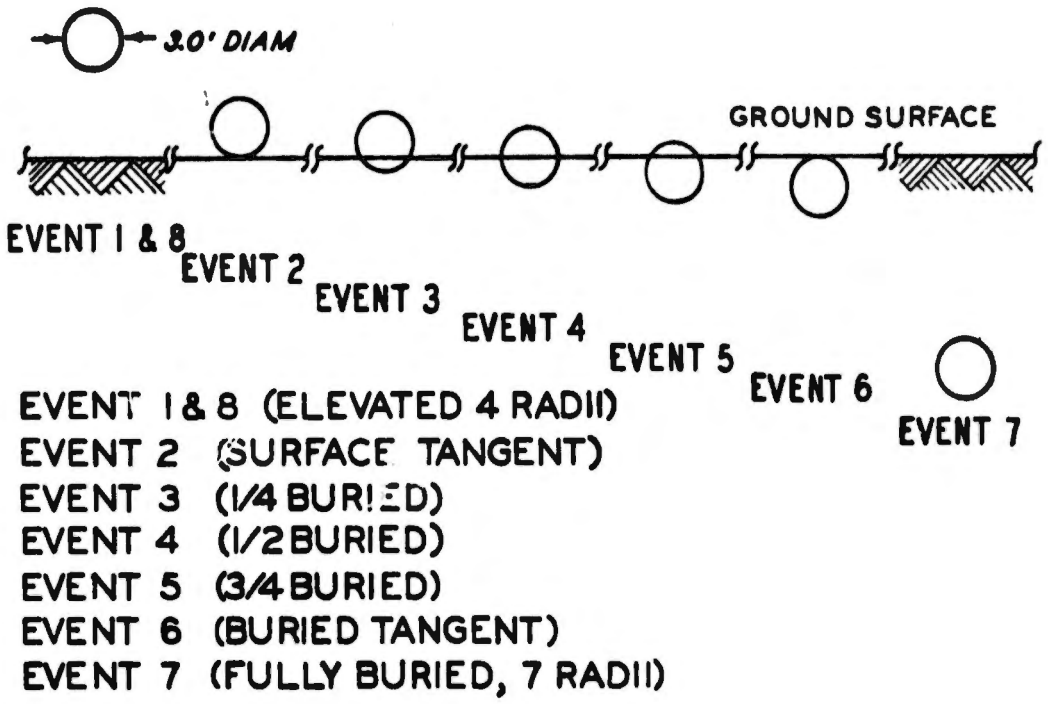

Figure 4. CENSE series 1000-lb nitromethane DOB test configurations

SPHERICAL CHARGE DOB TEST CONFIGURATIONS			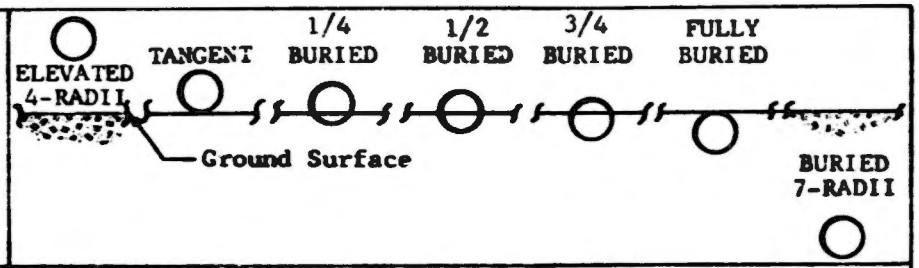						
TOTAL TESTS	EXPLOSIVE CHARGE		NUMBER OF EVENTS						
	Type	lb							
2	nitromethane	1000	2						
1	nitromethane	1000		1					
1	nitromethane	1000			1				
1	nitromethane	1000				1			
1	nitromethane	1000					1		
1	nitromethane	1000						1	
1	nitromethane	1000							1
12	C-4	1		3	1	2	1	5	
3	C-4	4			1	1		1	
2	C-4	8		1			1		
1	C-4	18		1					
2	C-4	27				1		1	

Figure 5. Explosive tests conducted

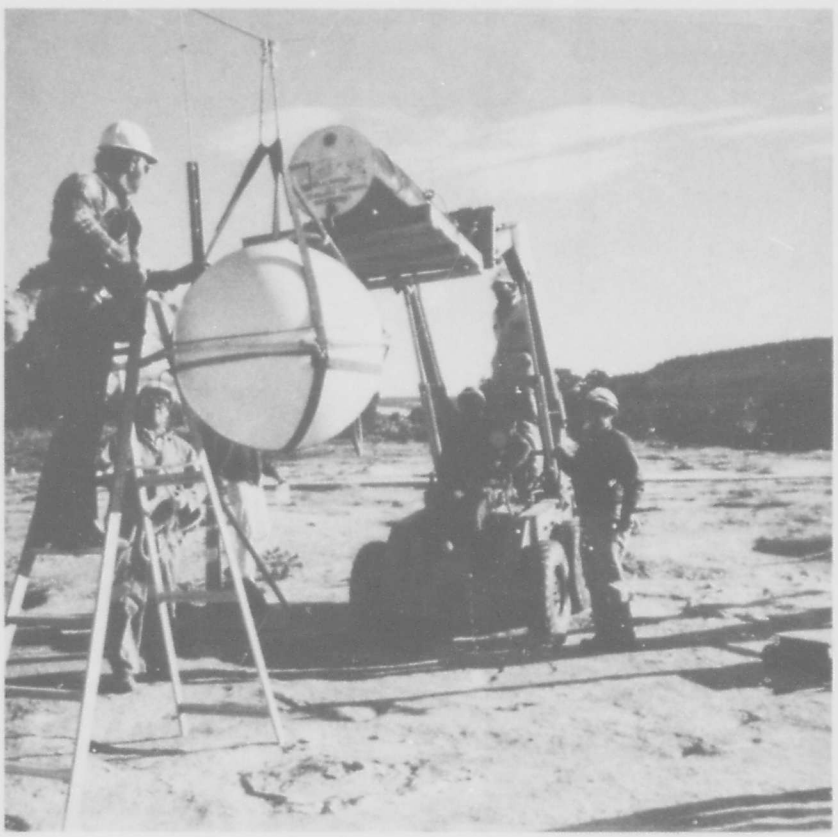

Figure 6. Typical loading operation of 1000-lb nitromethane charges

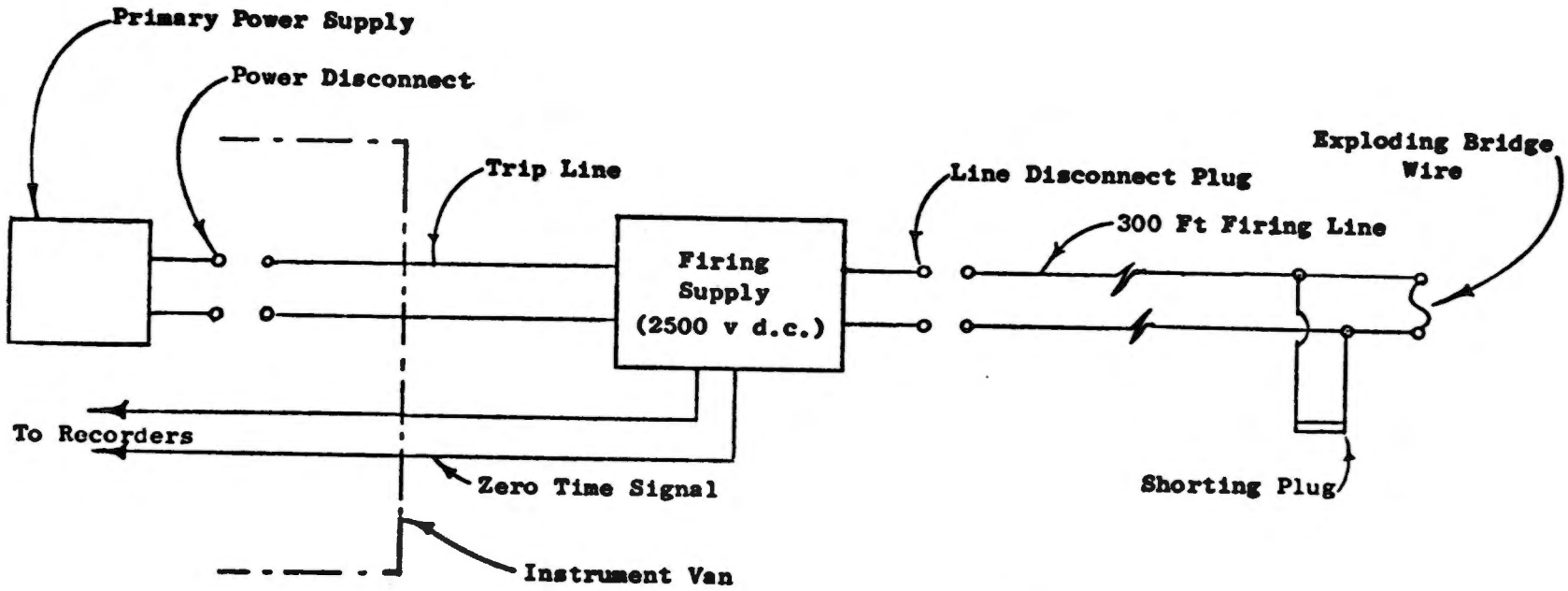

Figure 7. Exploding bridge wire firing circuit diagram

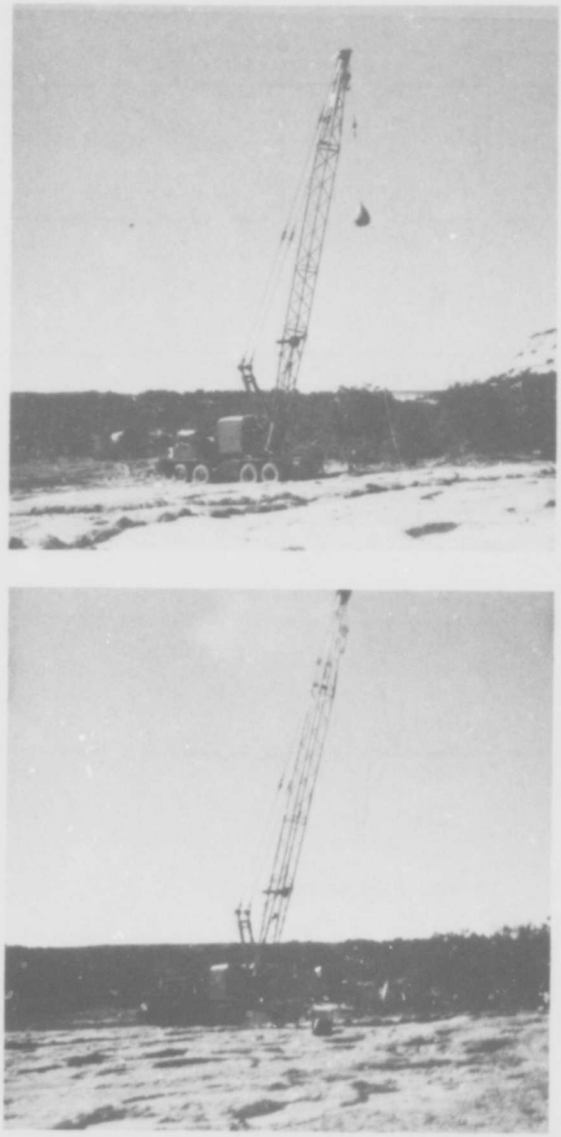

Figure 8. Views of a typical impact test

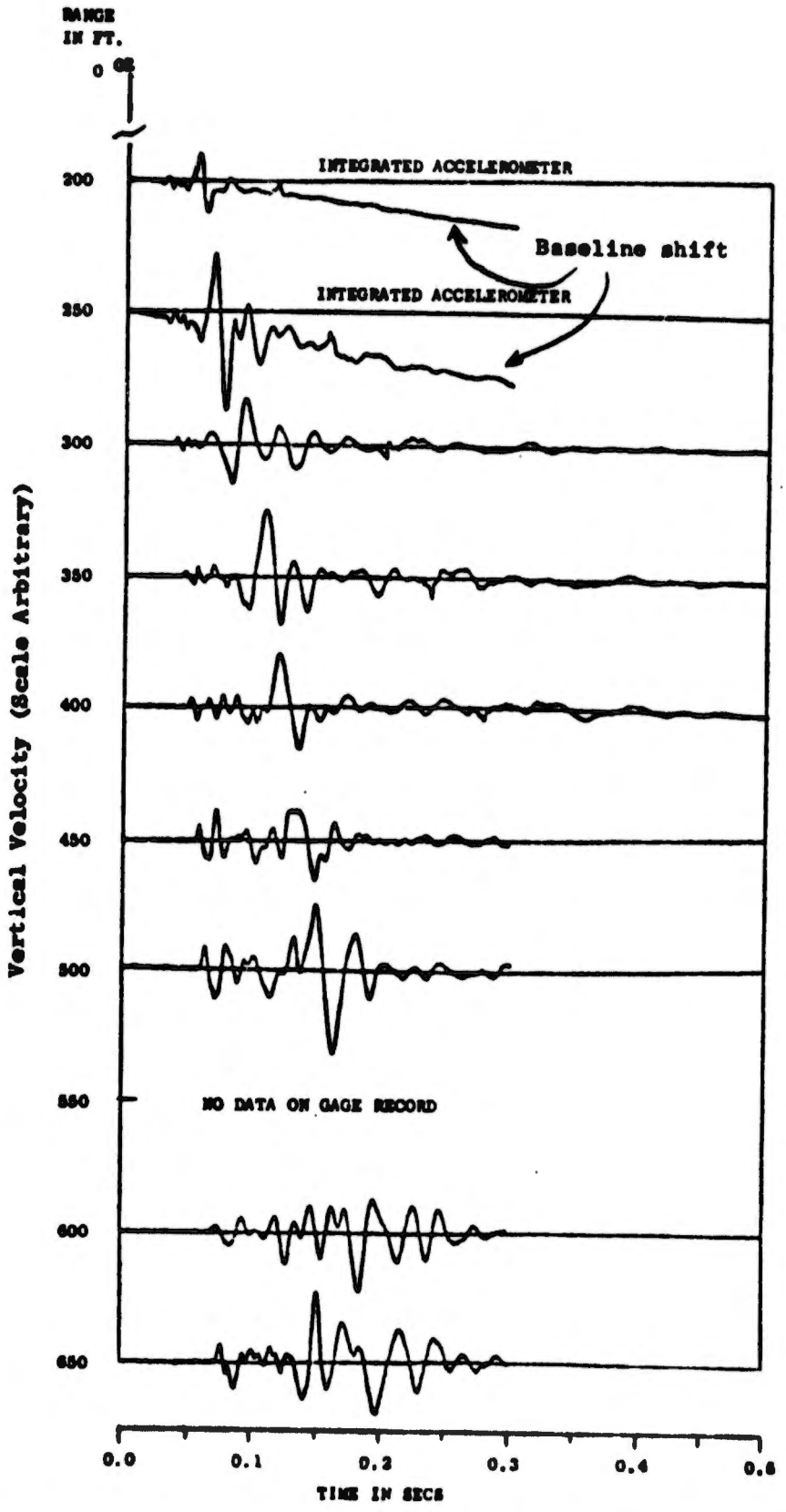

Figure 9. Typical CENSE vertical velocity-time history, 1000-lb, four-charge radii above ground

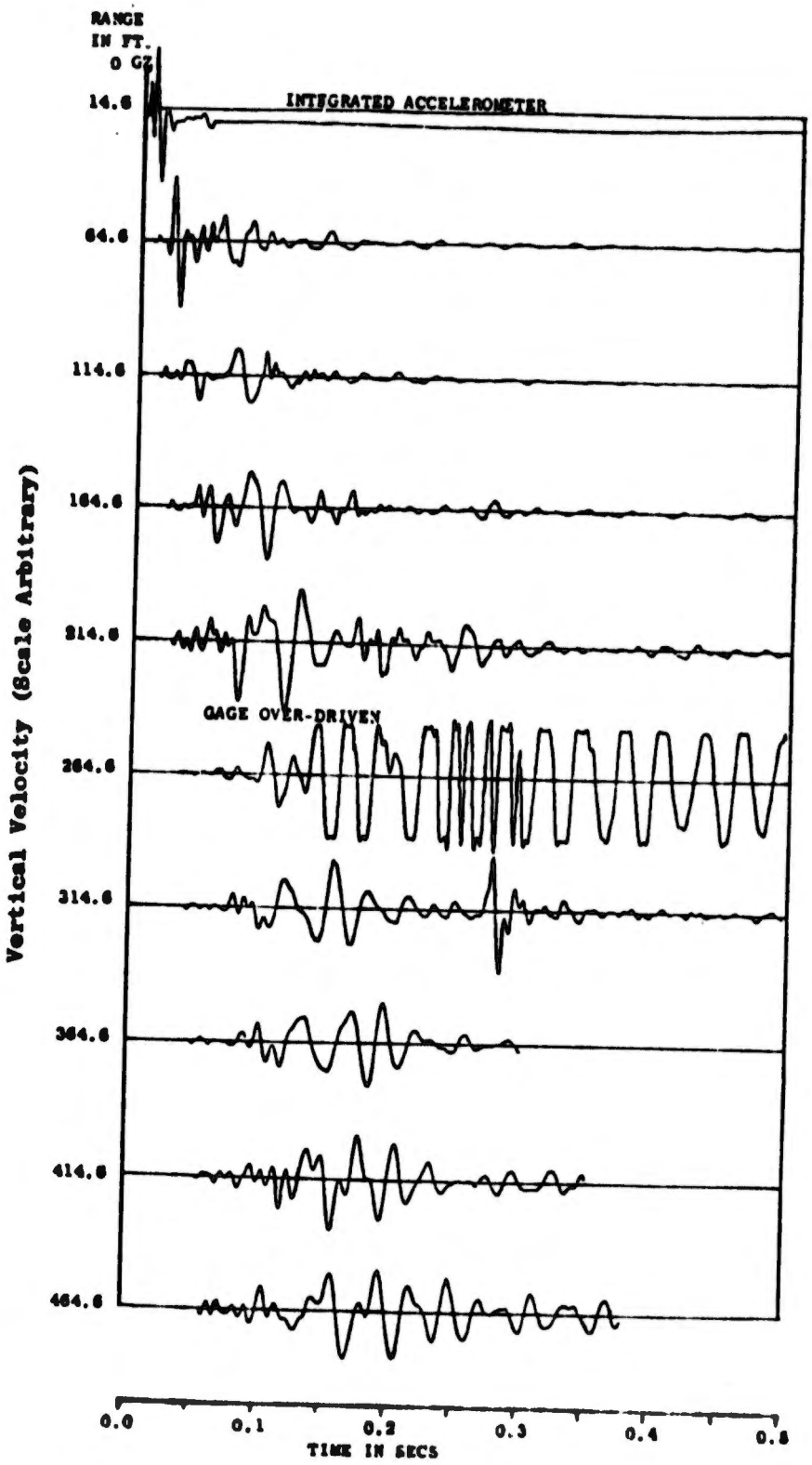

Figure 10. Typical SHE vertical velocity-time history, 1-lb surface tangent

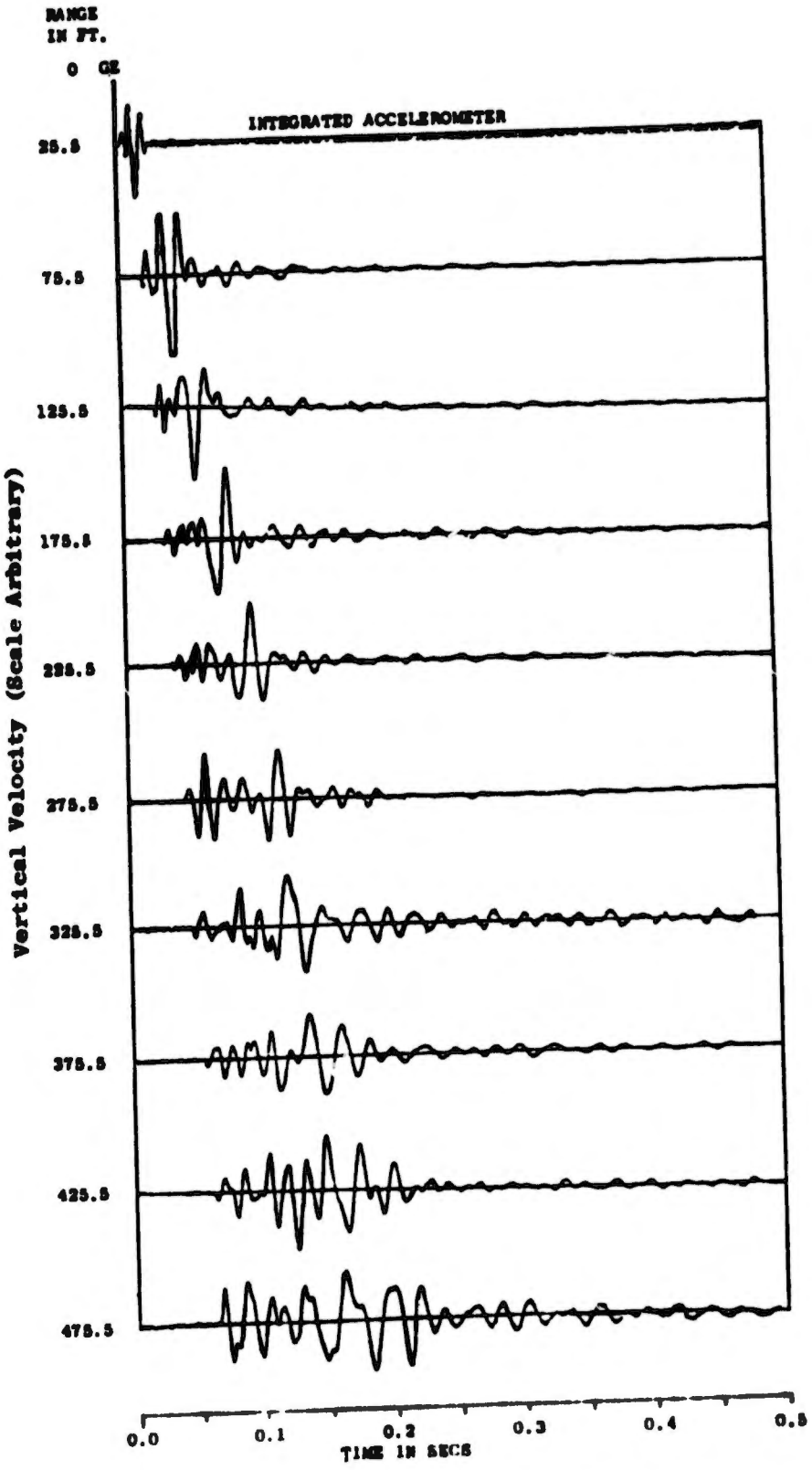

Figure 11. Typical SMIT vertical velocity-time history, W = 6800 lb , h = 40 ft

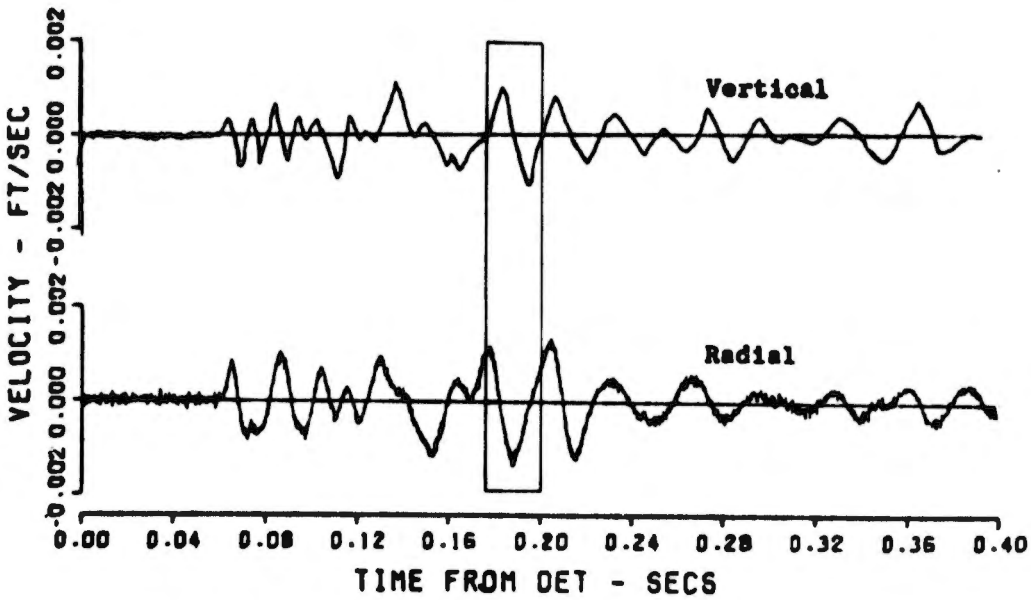

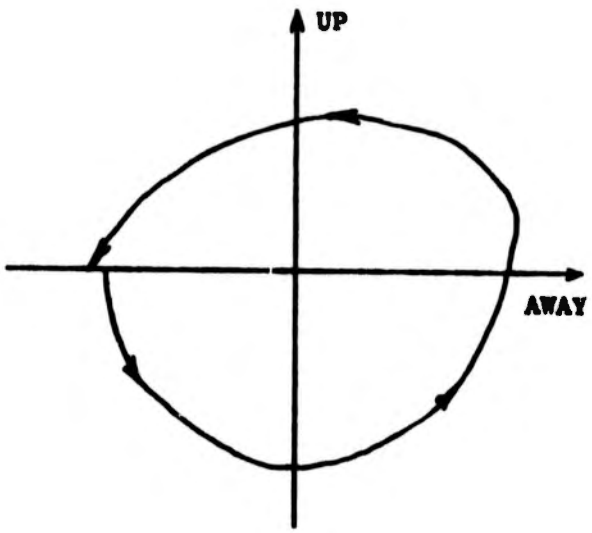

Figure 12. Typical explosion-produced particle motion path

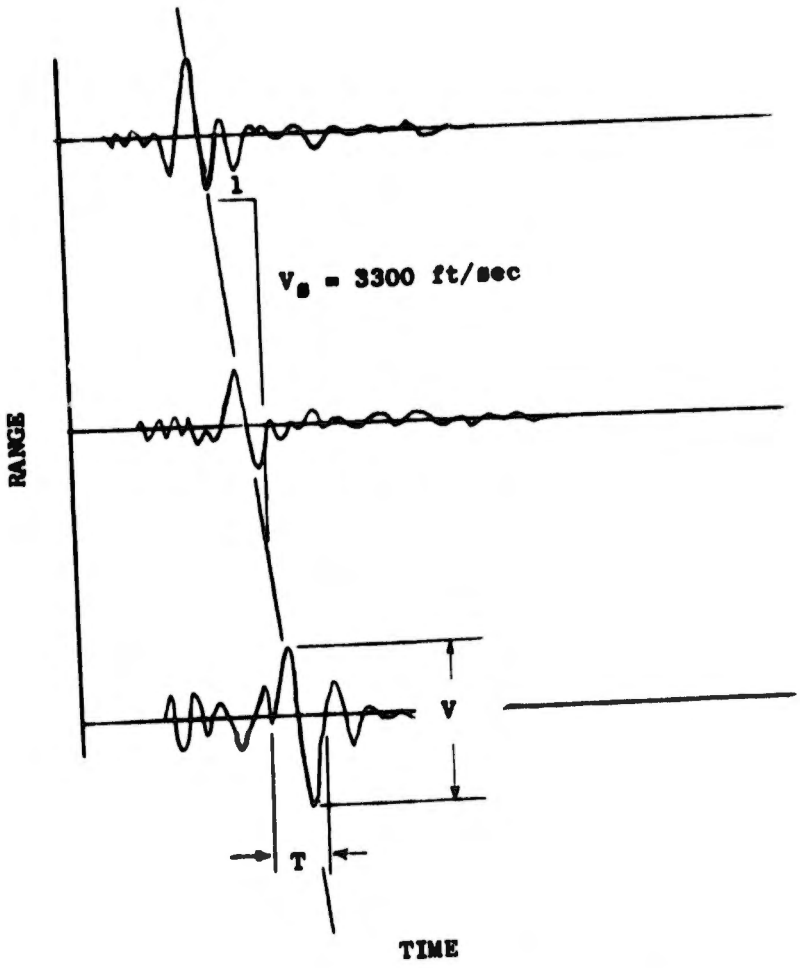

Figure 13. Seismic descriptors used in plots

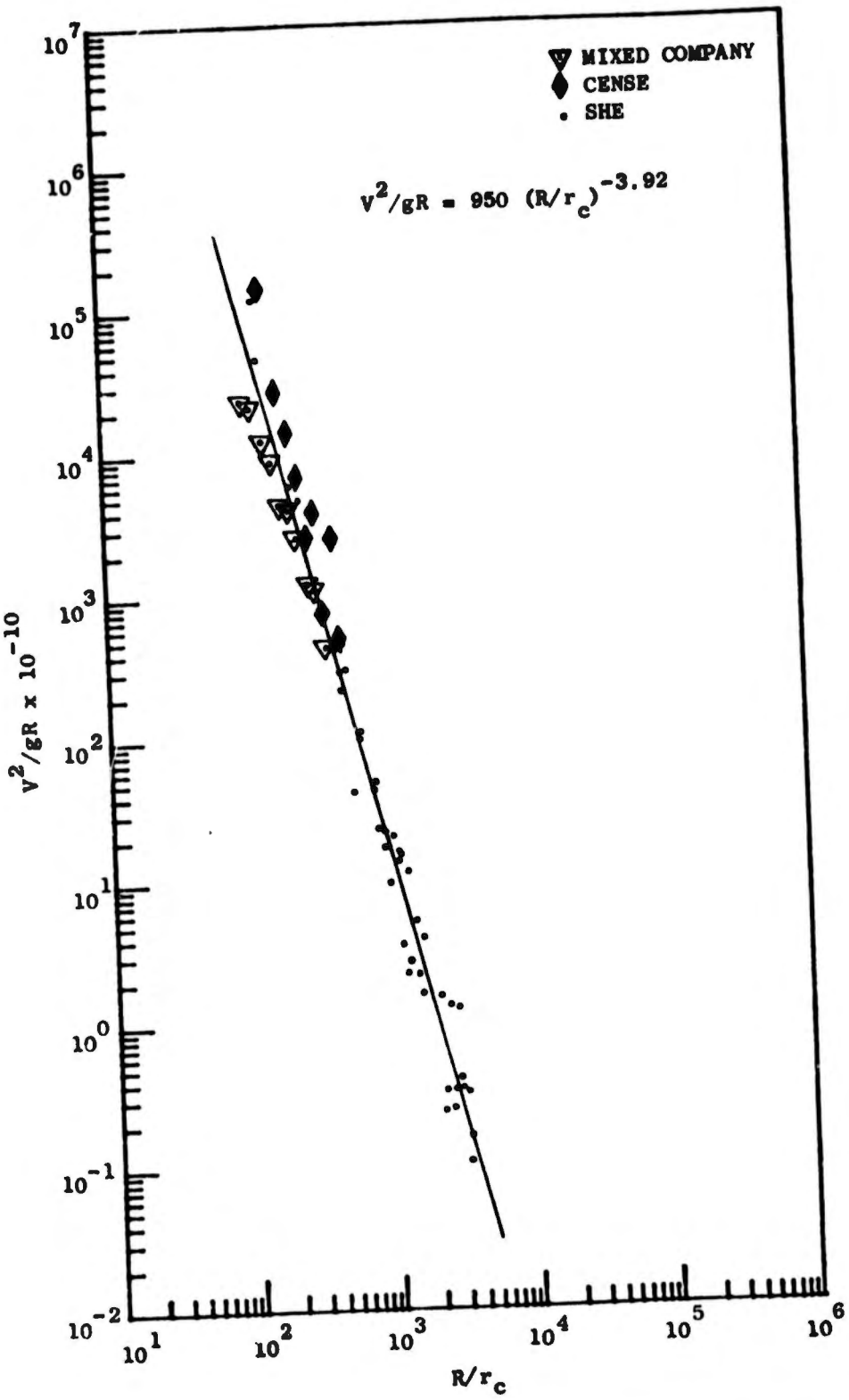

Figure 14. Normalized vertical peak particle kinetic energy as a function of scaled range for surface-tangent HE shots

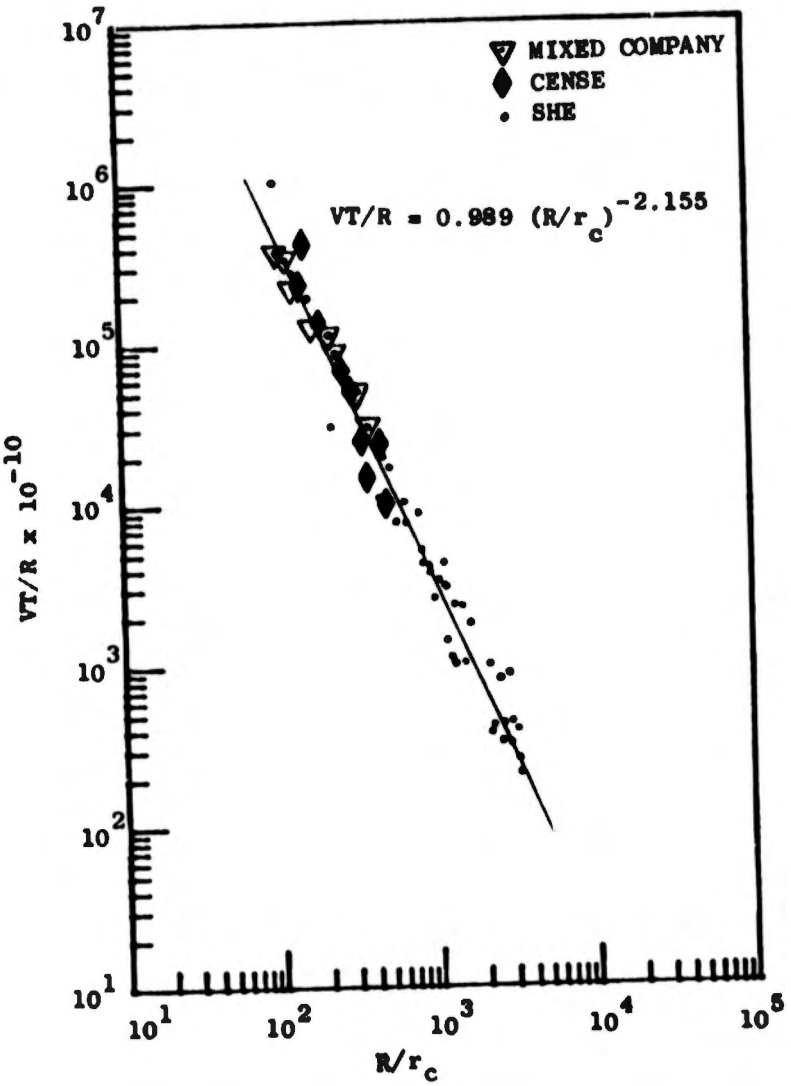

Figure 15. Normalized vertical particle displacement as a function of scaled range for surface-tangent HE shots

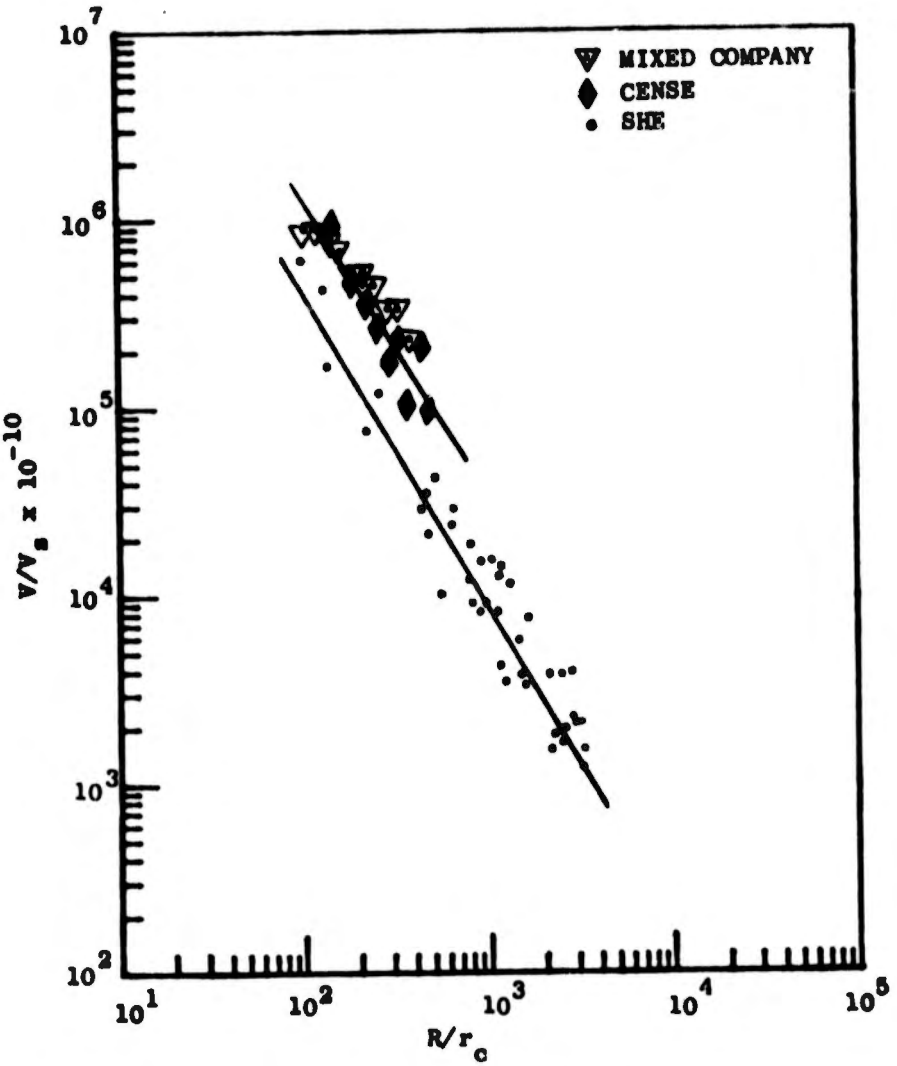

Figure 16. Normalized peak-to-peak vertical velocity as a function of scaled range for surface-tangent HE shots

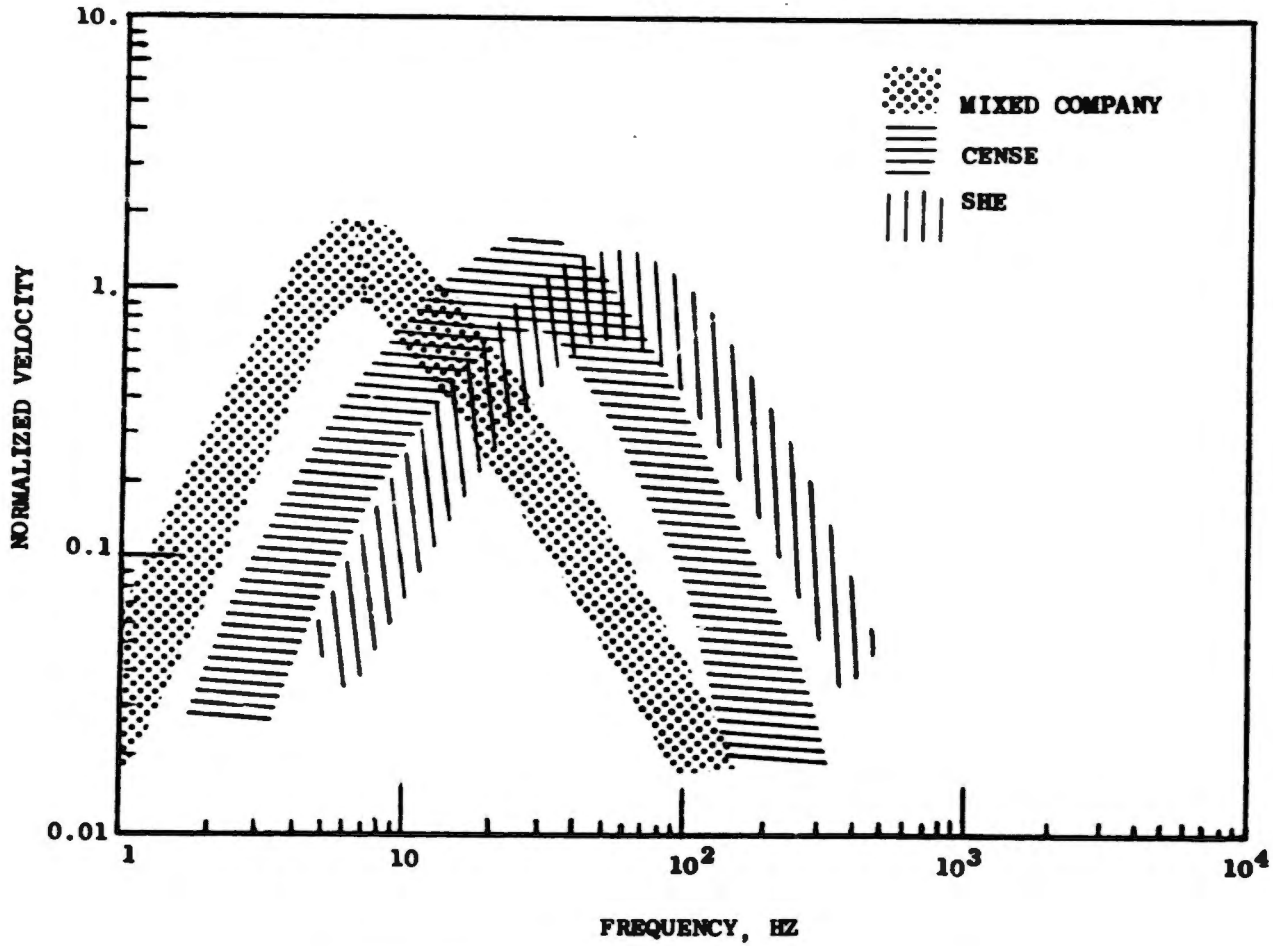

Figure 17. Comparison of vertical spectra for explosive events

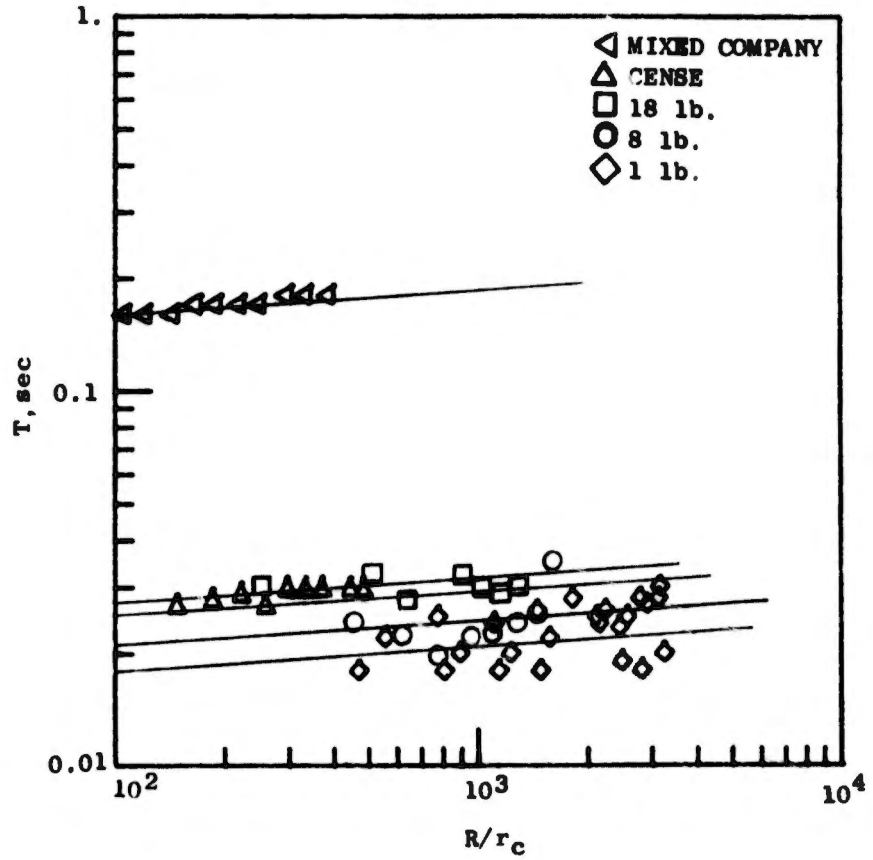

Figure 18. Vertical period as a function of scaled range

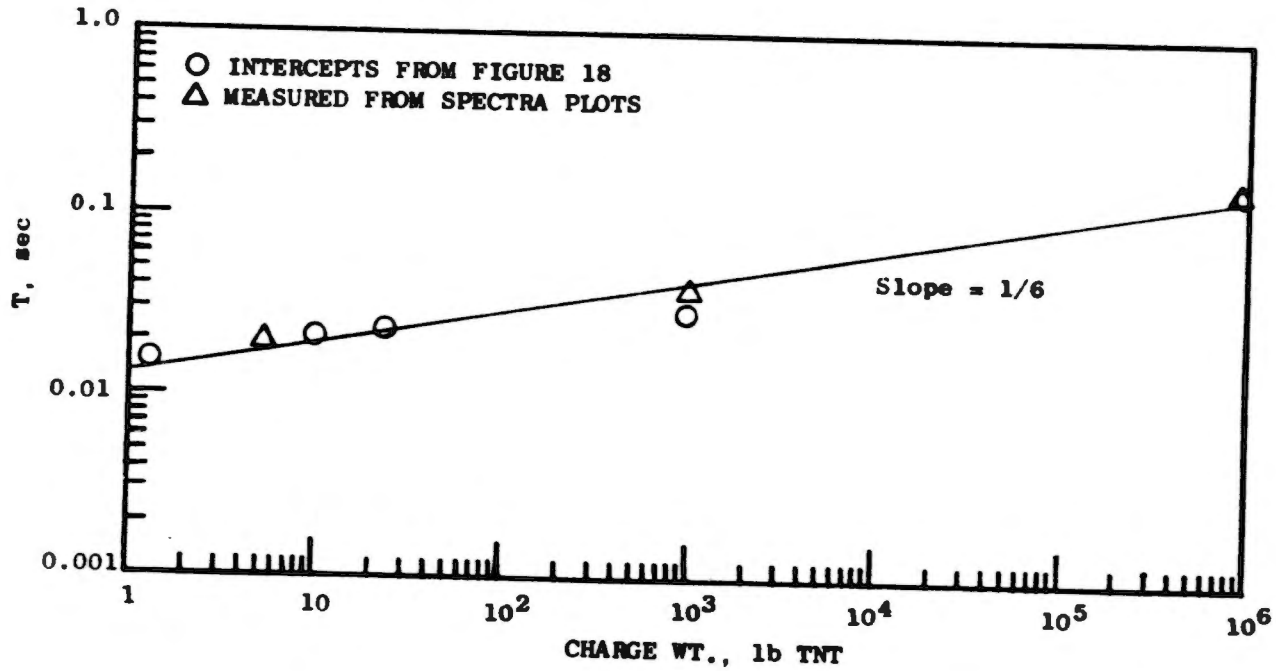

Figure 19. Period intercepts at a scaled range of 100 as a function of charge weight

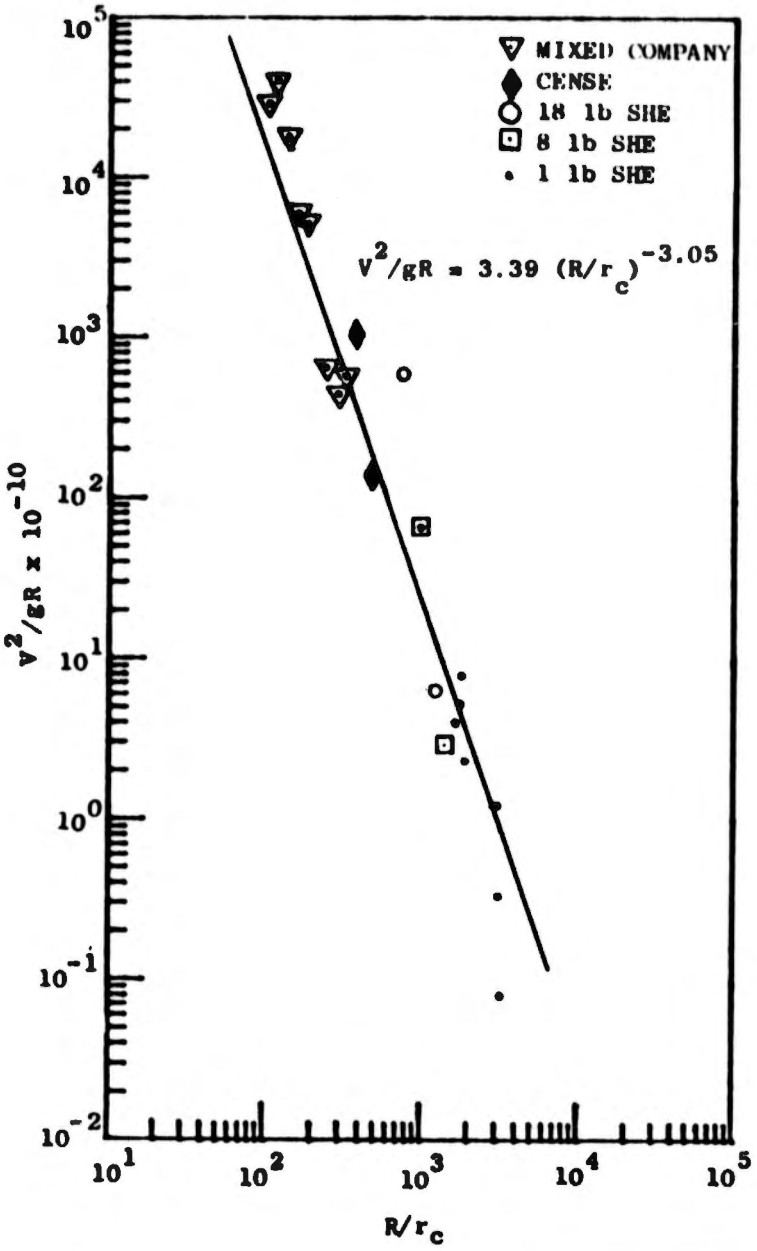

Figure 20. Normalized radial peak particle kinetic energy as a function of scaled range for surface-tangent HE shots

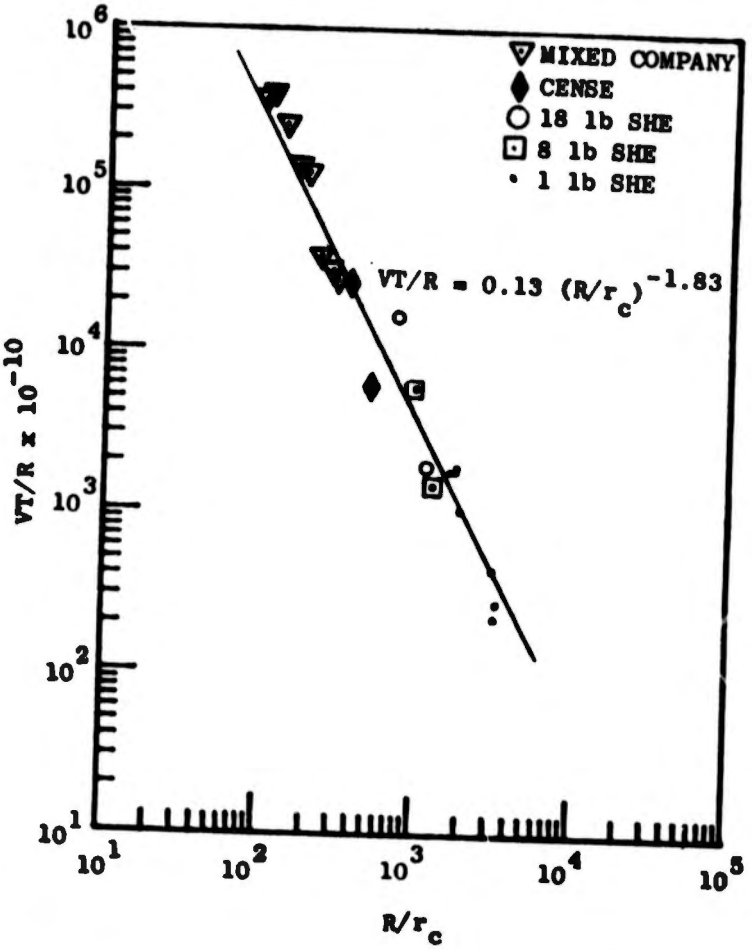

Figure 21. Normalized radial particle displacement as a function of scaled range for surface-tangent HE shots

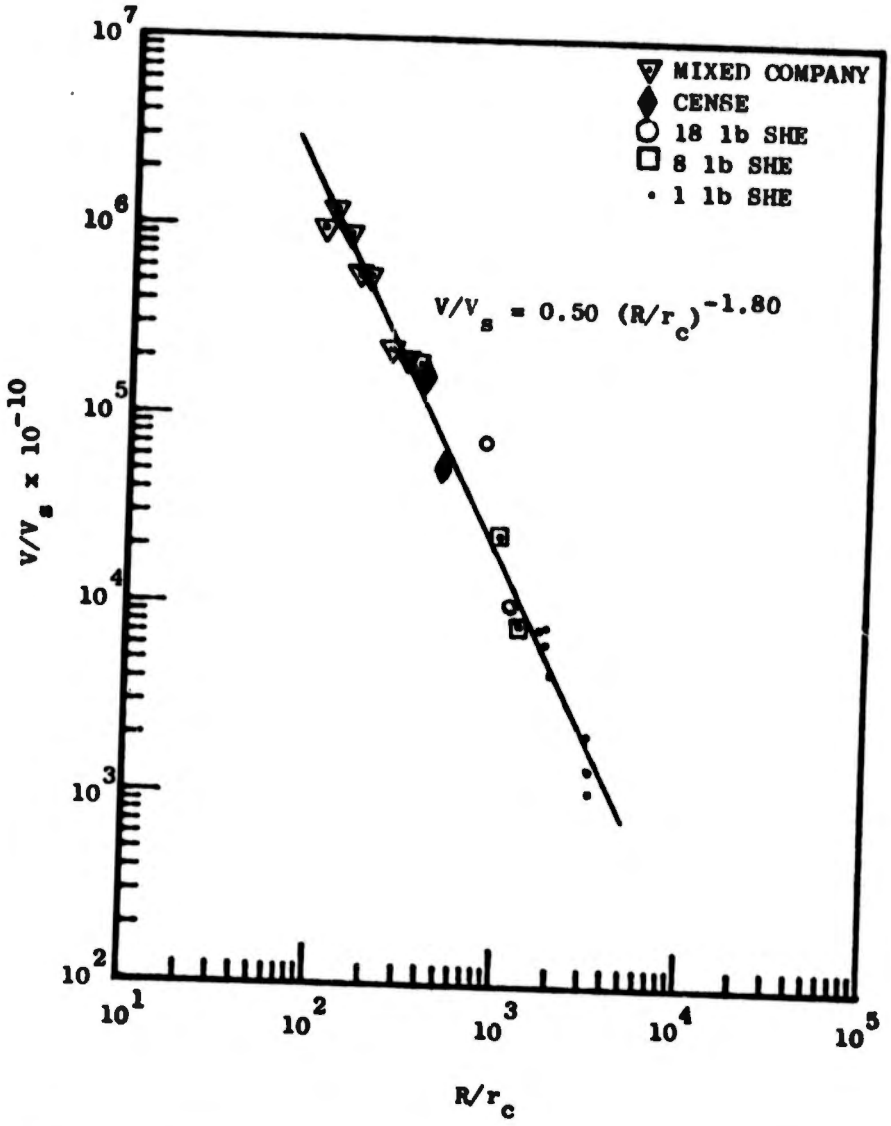

Figure 22. Normalized peak-to-peak radial velocity as a function of scaled range for surface-tangent HE shots

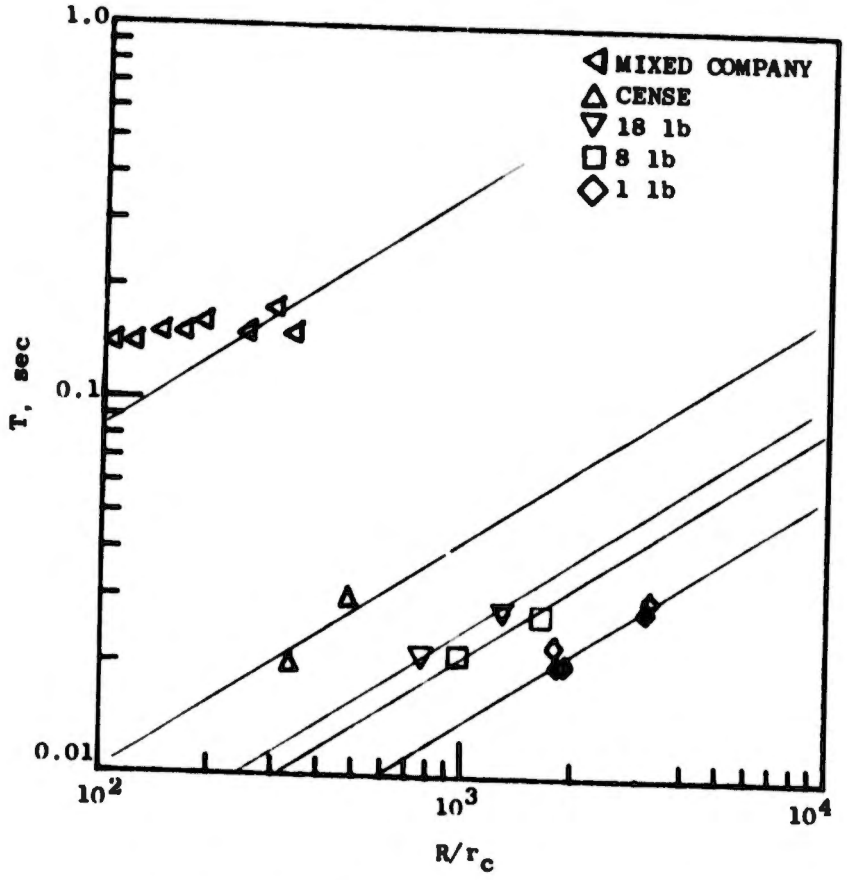

Figure 23. Radial period as a function of scaled range

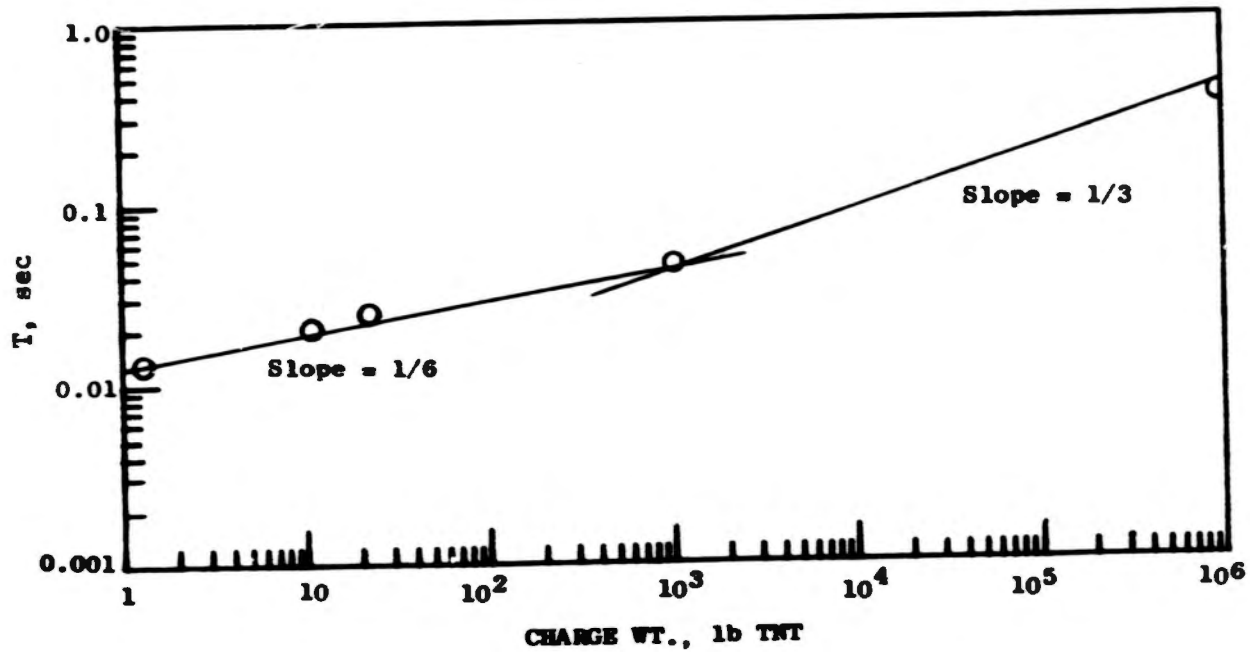

Figure 24. Period intercepts at a scaled range of 1000 as a function of charge weight

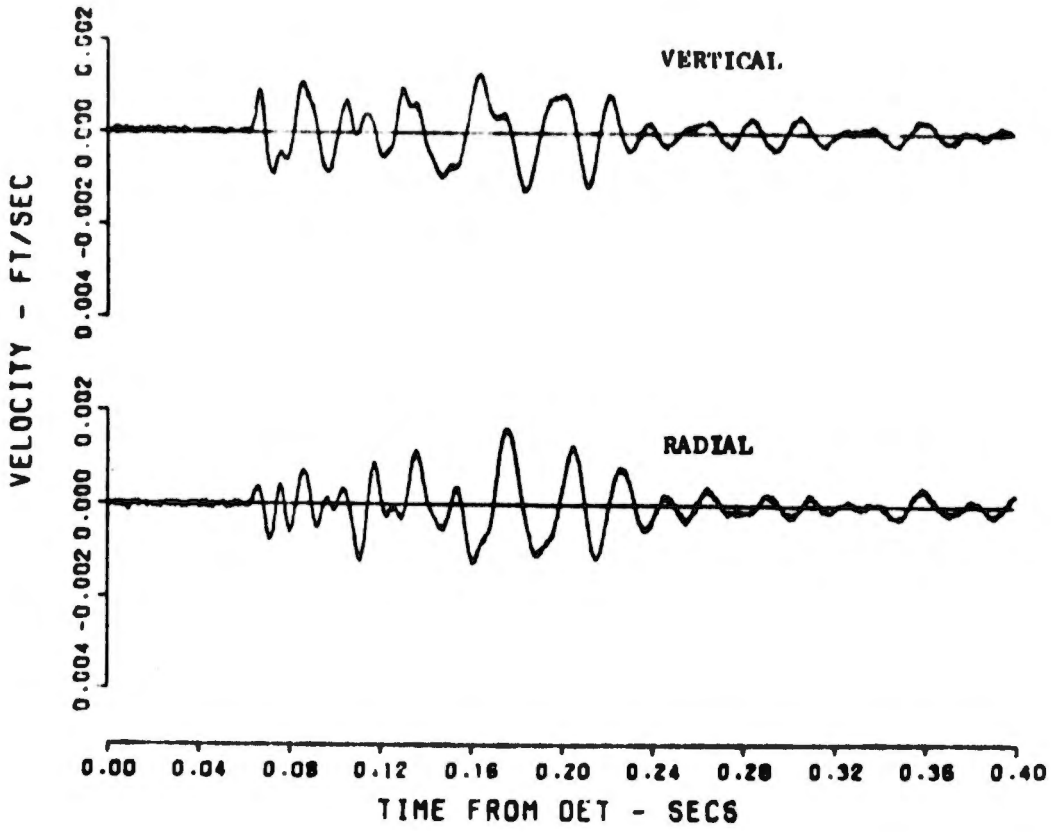

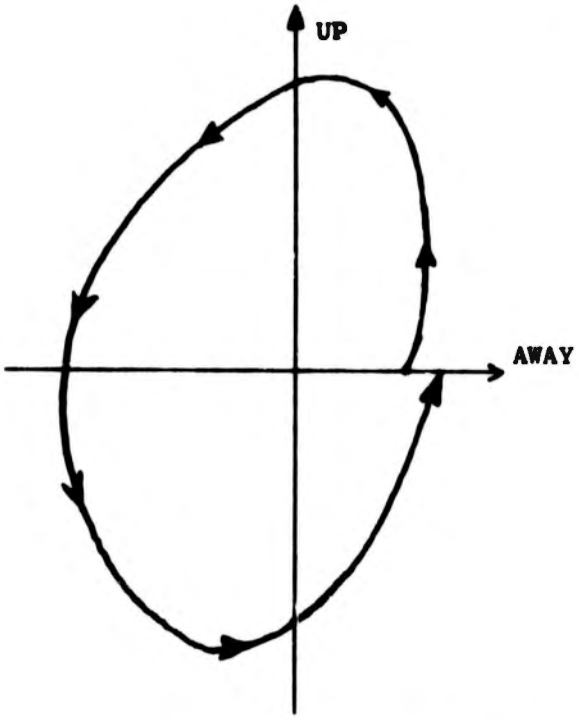

Figure 26. Typical impact-produced particle motion path

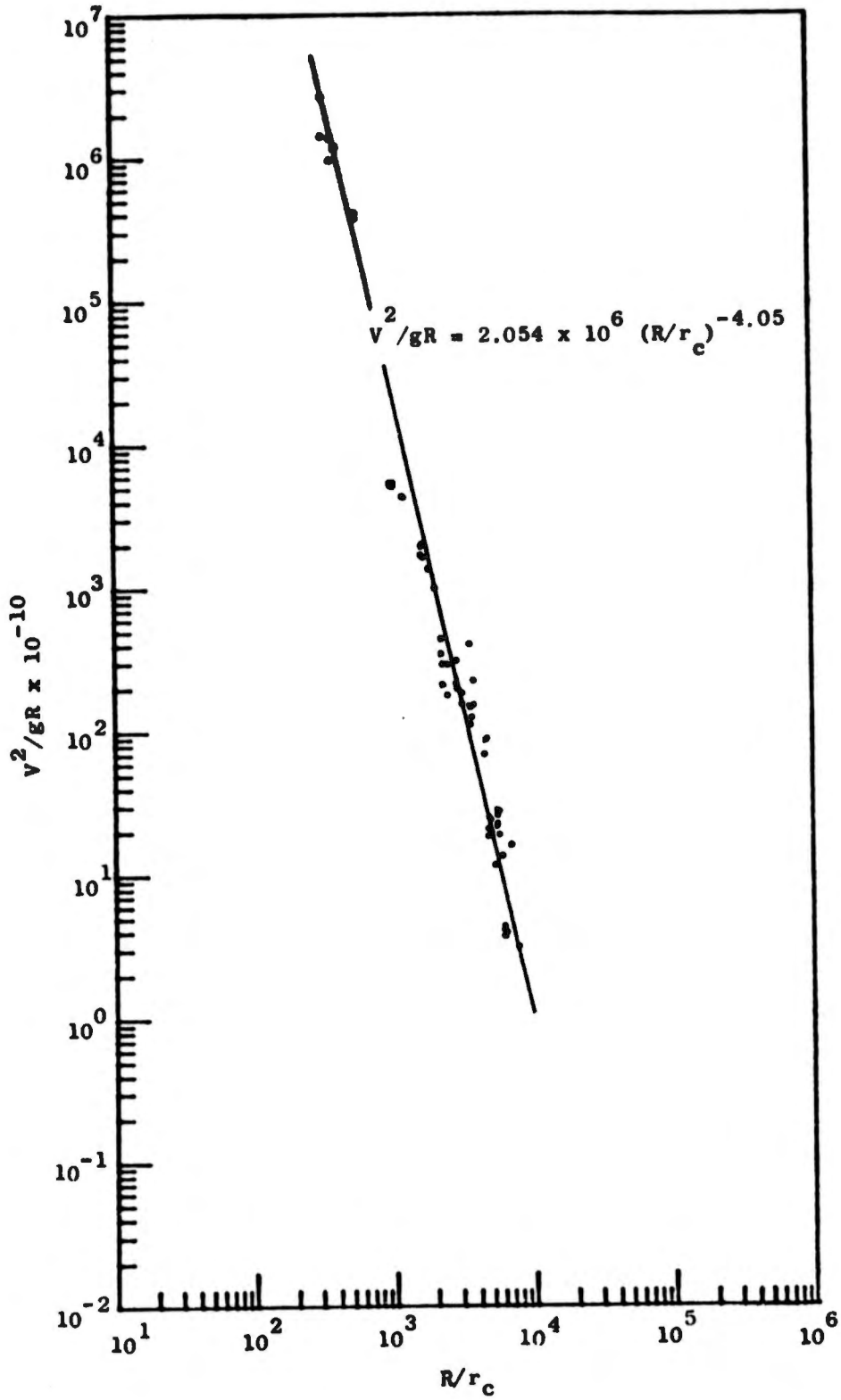

Figure 26. Normalized vertical peak particle kinetic energy as a function of scaled range for SMIT test series

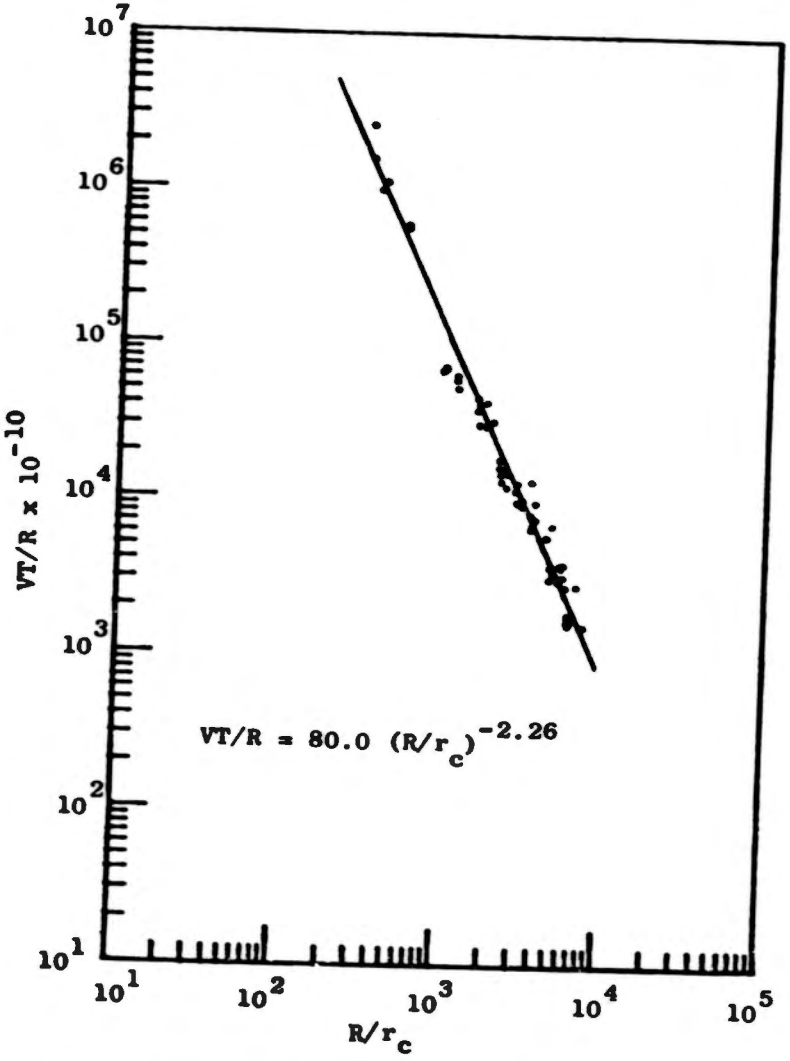

Figure 27. Normalized vertical particle displacement as a function of scaled range for SMIT test series

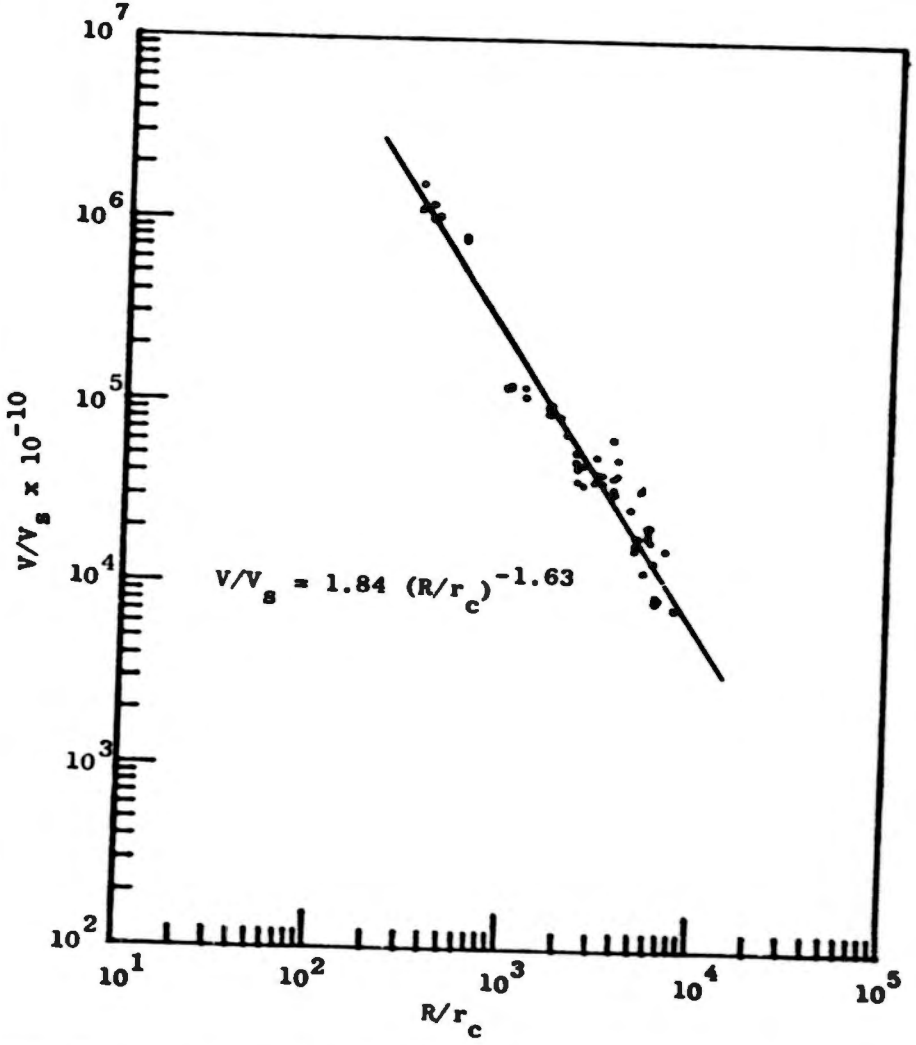

Figure 28. Normalized peak-to-peak vertical velocity as a function of scaled range for SMIT test series

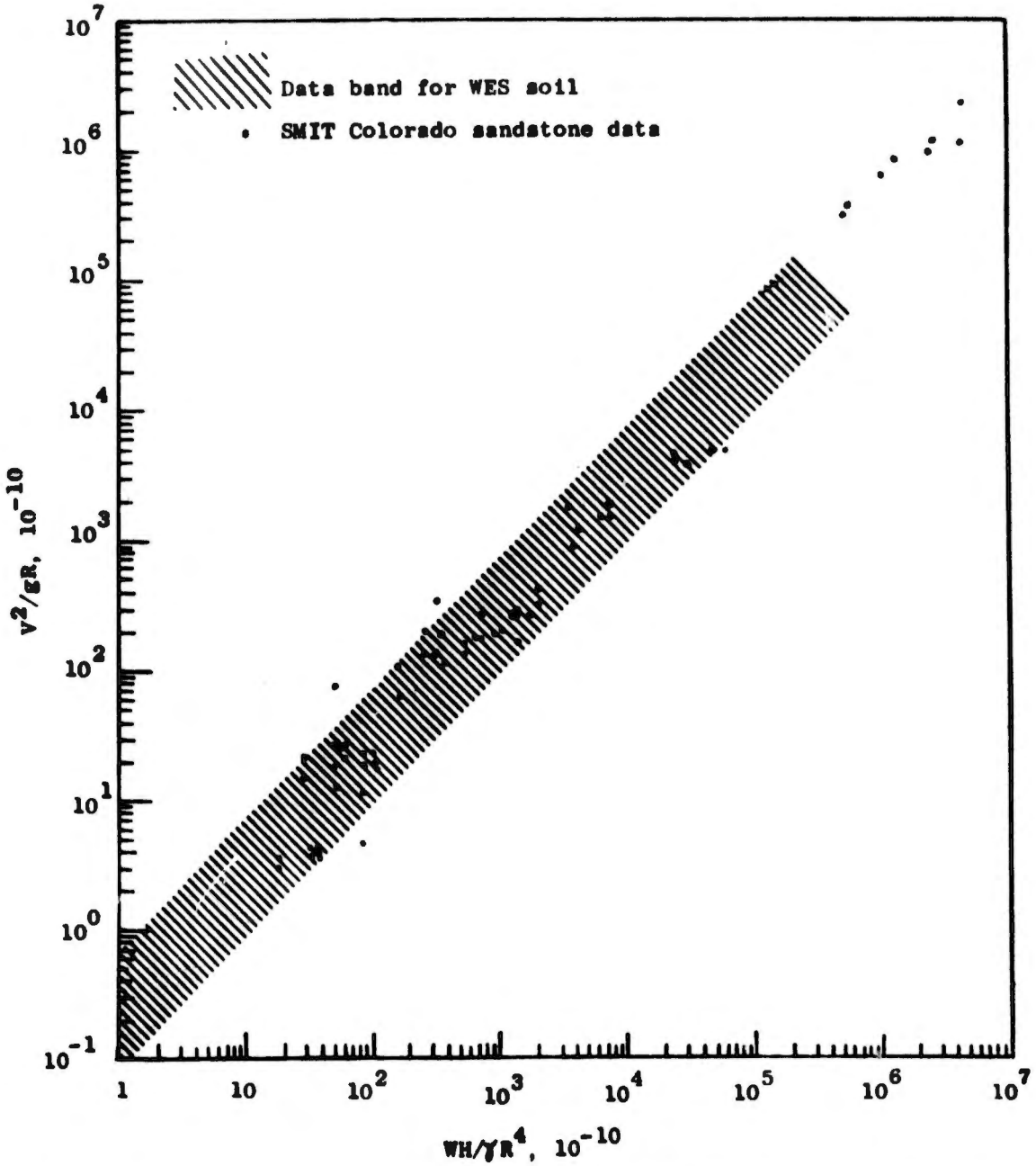

Figure 40. Normalized vertical peak particle kinetic energy as a function of normalized potential energy

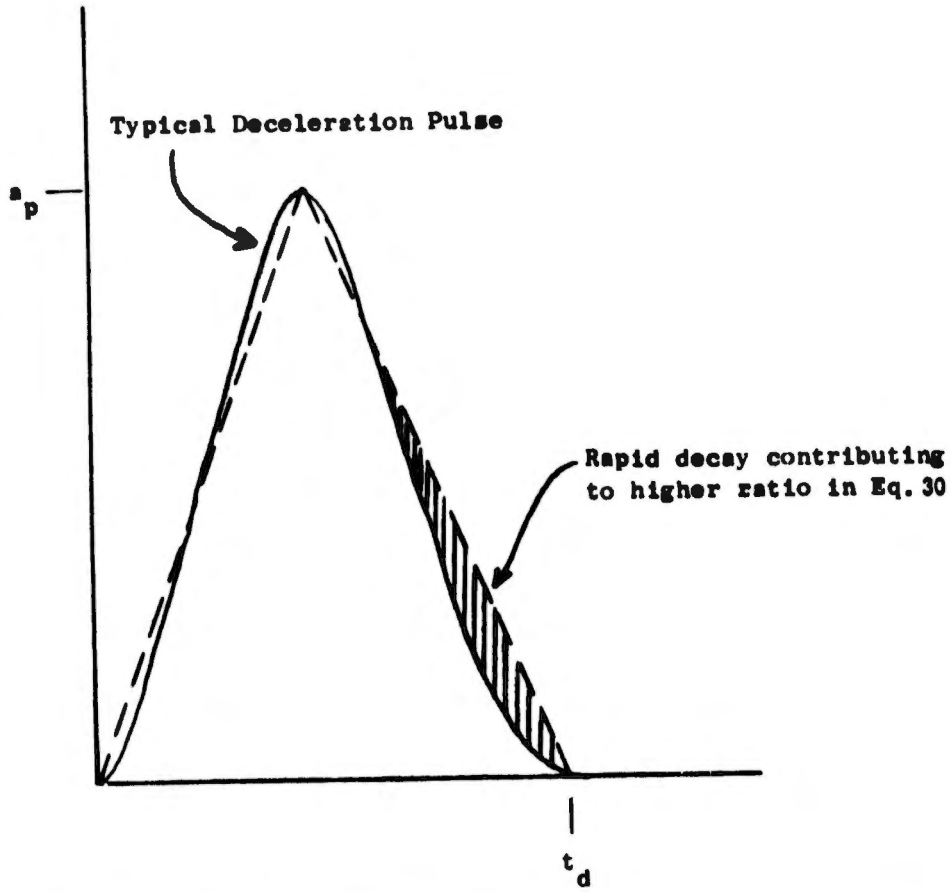

Figure 39. Typical sphere deceleration pulse compared to triangular approximation

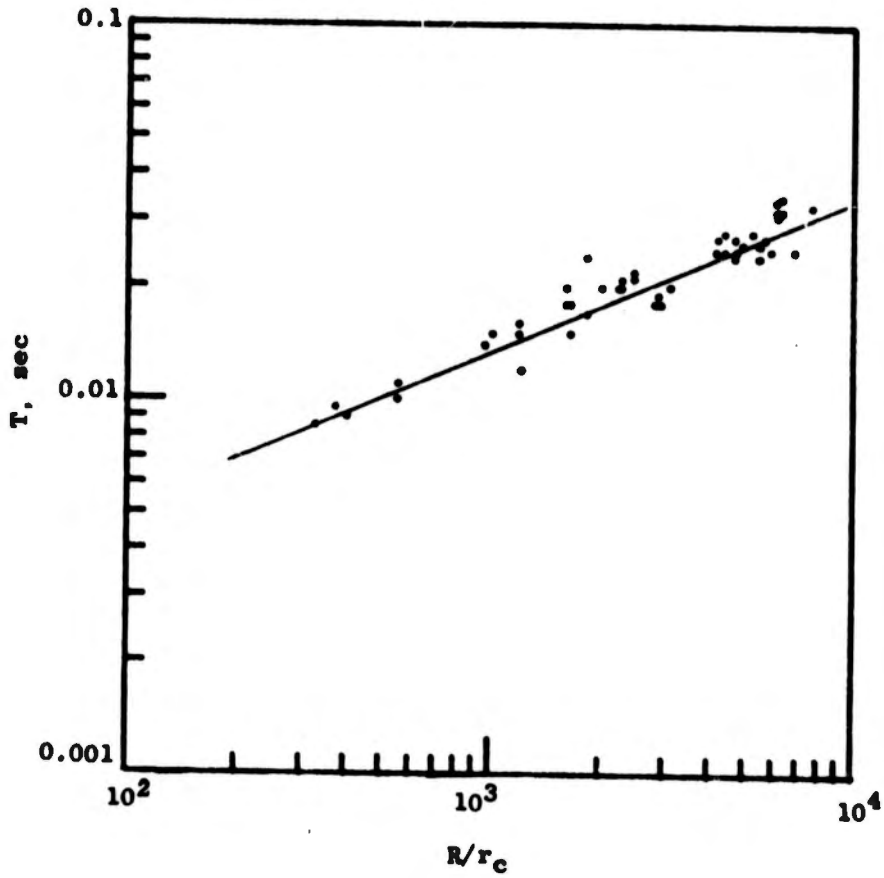

Figure 29. Vertical period as a function of scaled range for SMIT test series

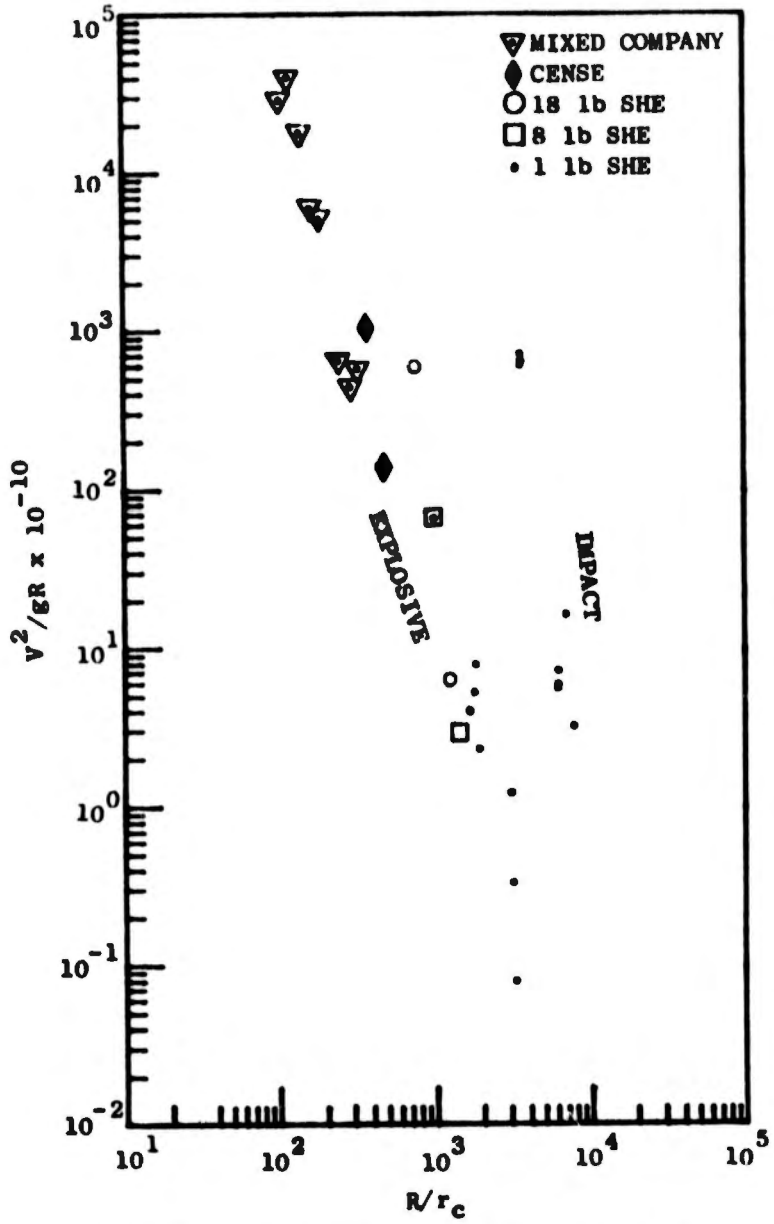

Figure 30. Normalized radial peak particle kinetic energy as a function of scaled range

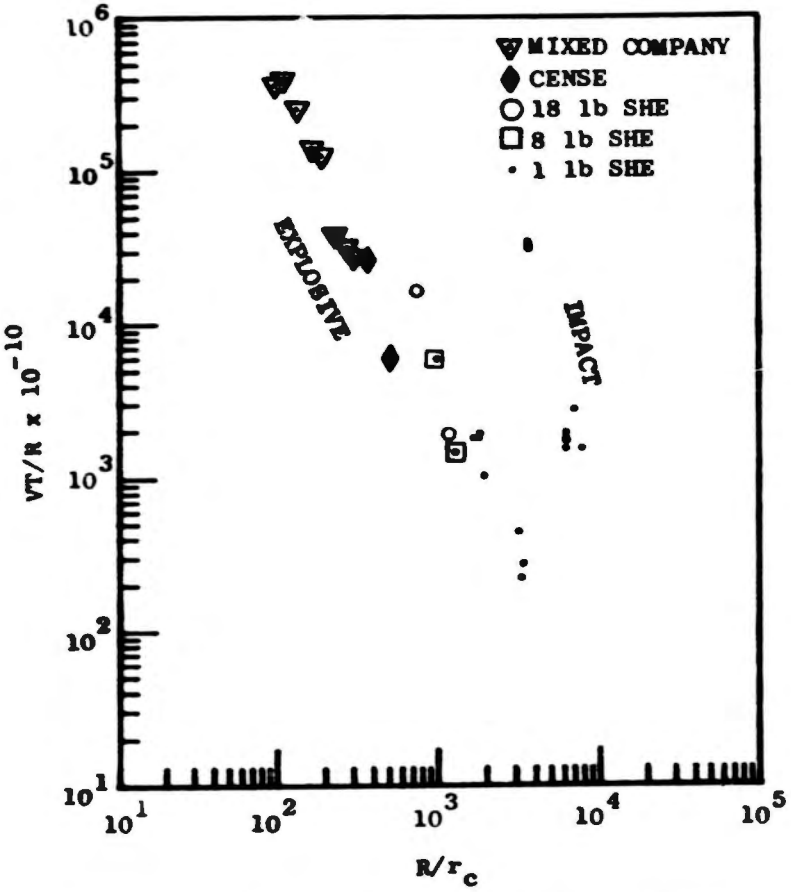

Figure 31. Normalized radial particle displacement as a function of scaled range

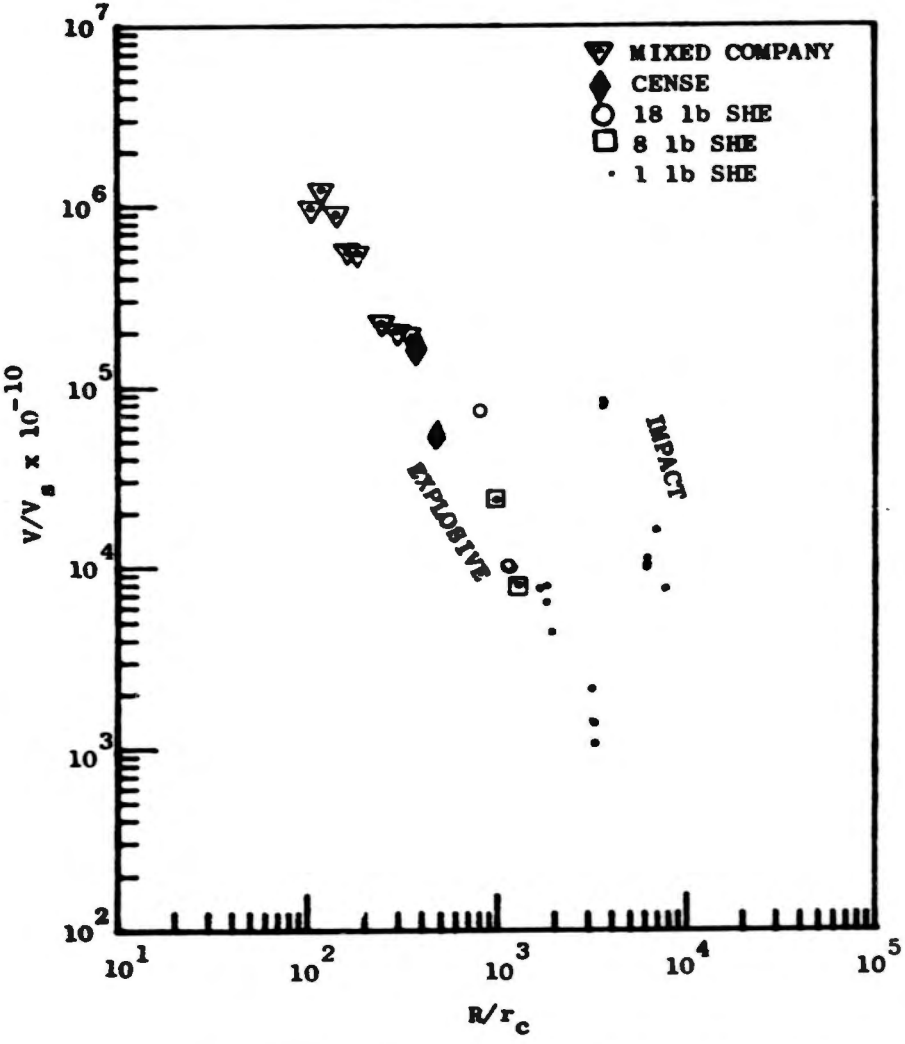

Figure 32. Normalized peak-to-peak radial velocity as a function of scaled range

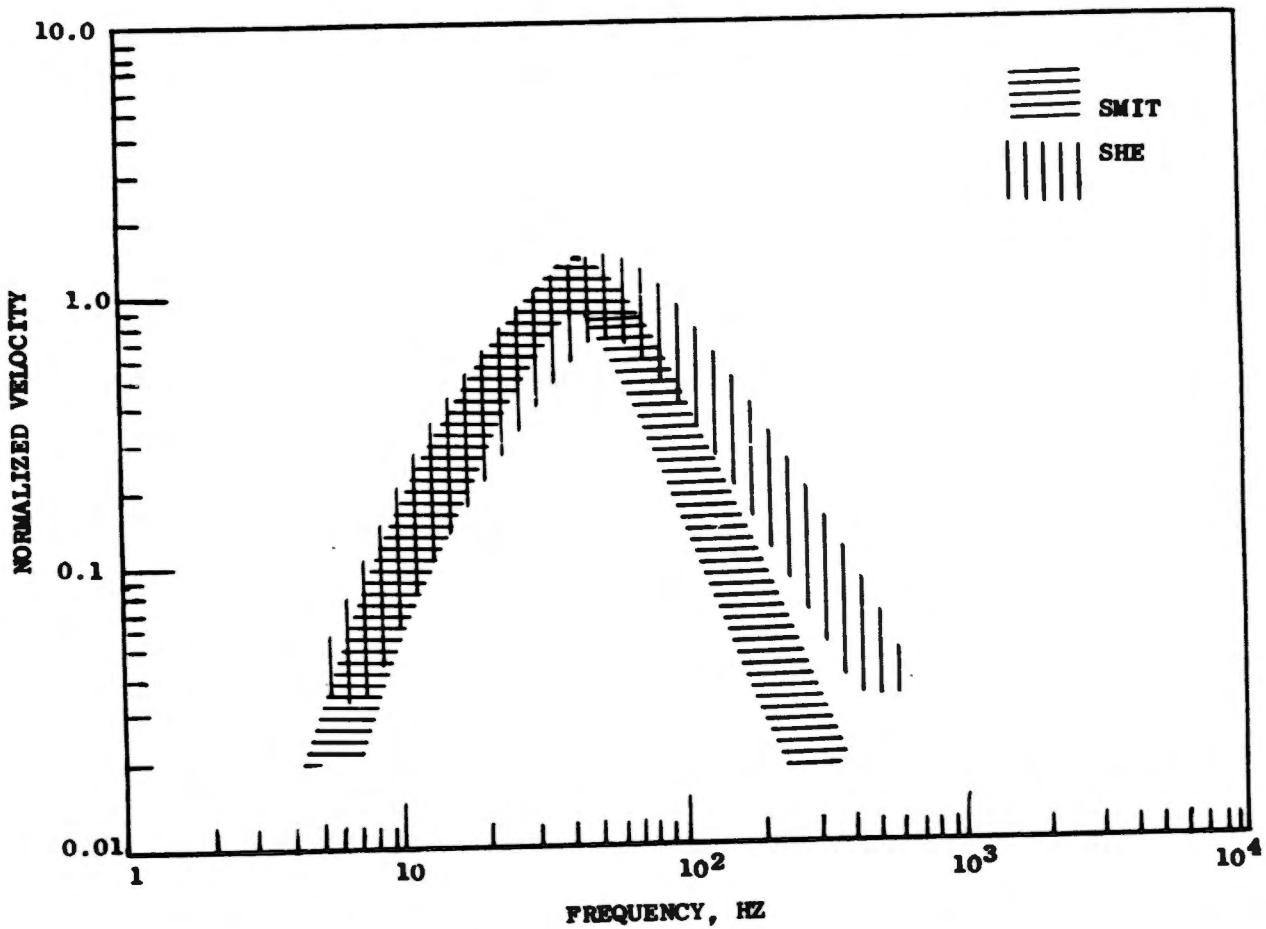

Figure 33. Comparison of vertical spectra for SMIT and SHE tests

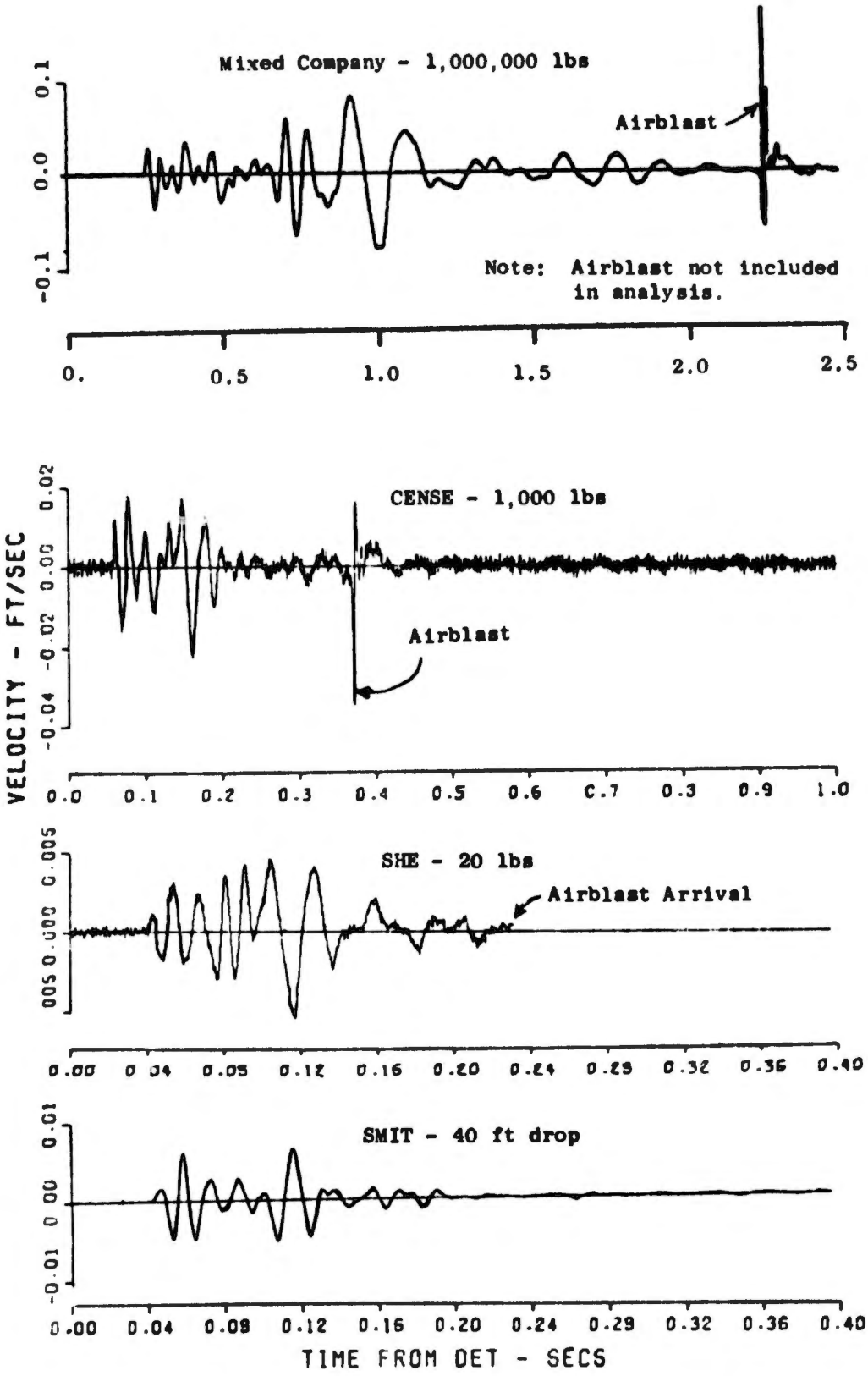

Figure 34. Comparison of vertical velocity wave forms of various explosive and impact events

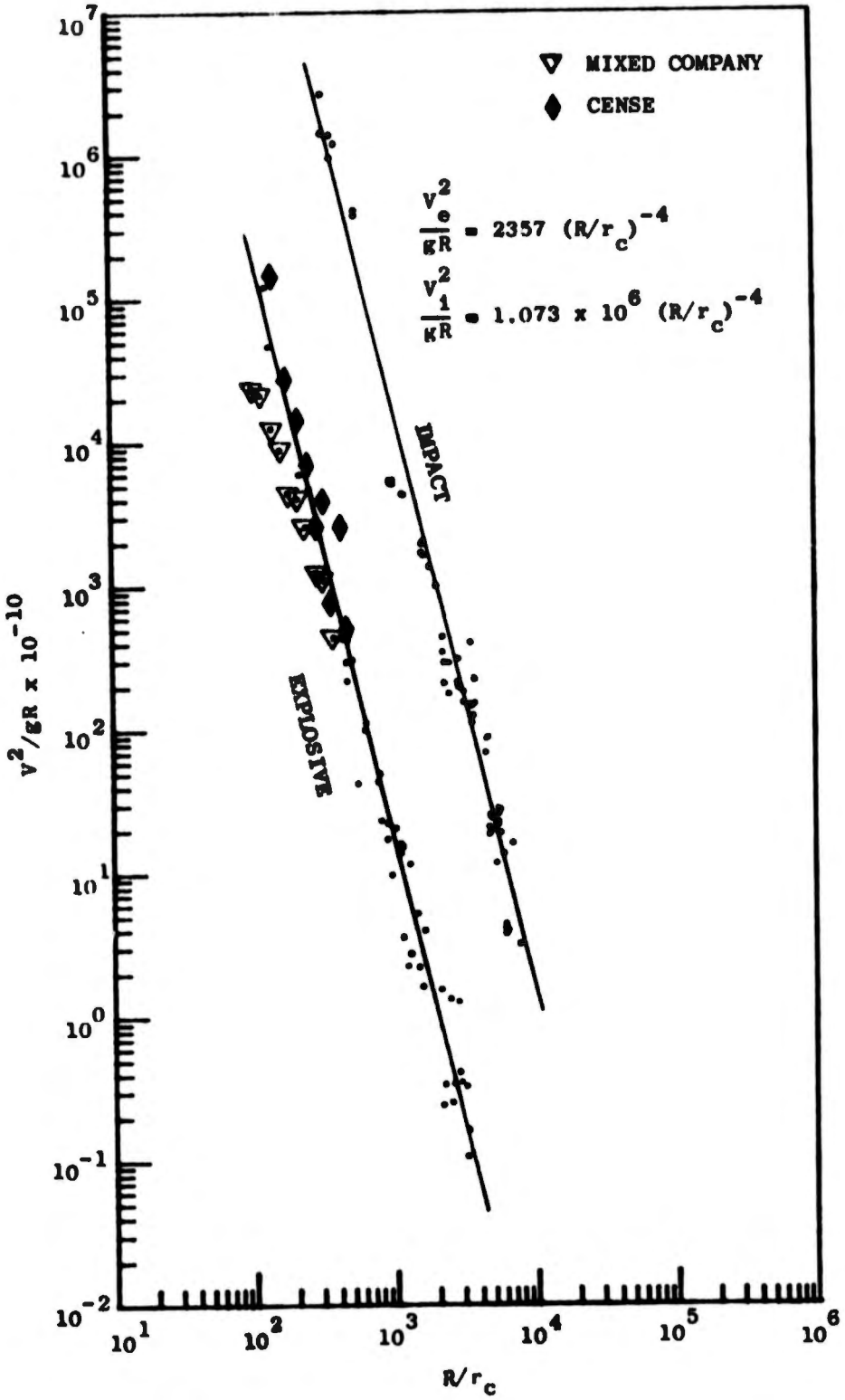

Figure 35. Normalized vertical peak particle kinetic energy as a function of scaled range

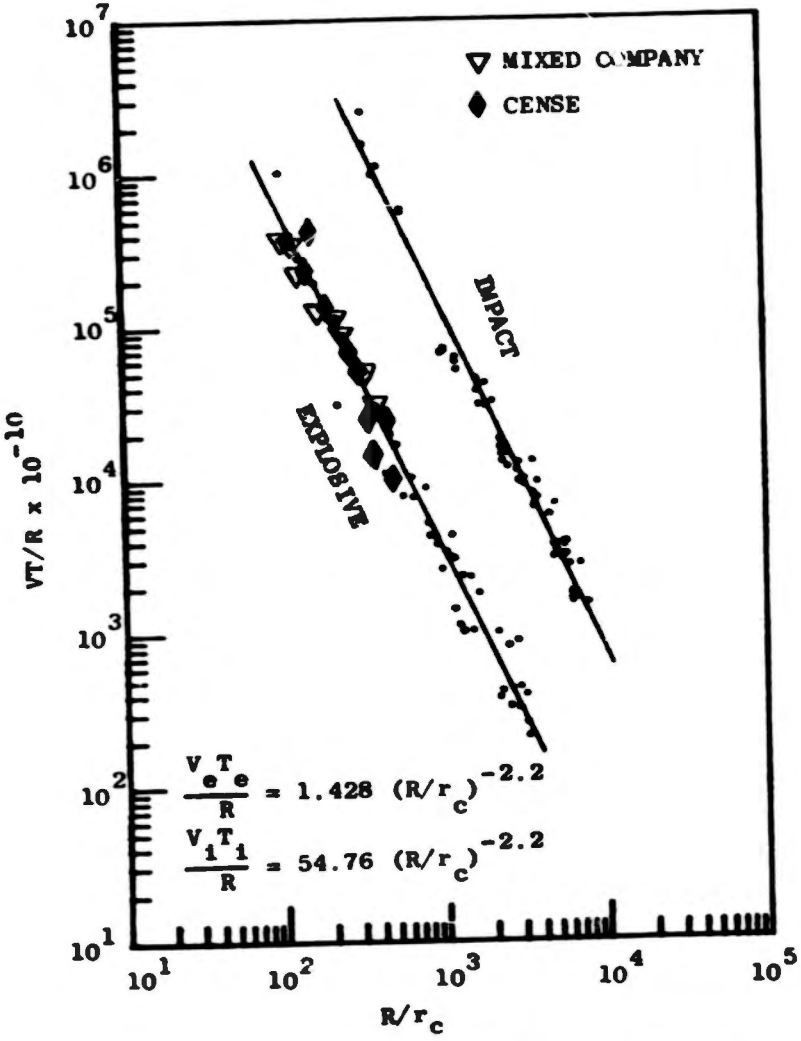

Figure 36. Normalized vertical particle displacement as a function of scaled range

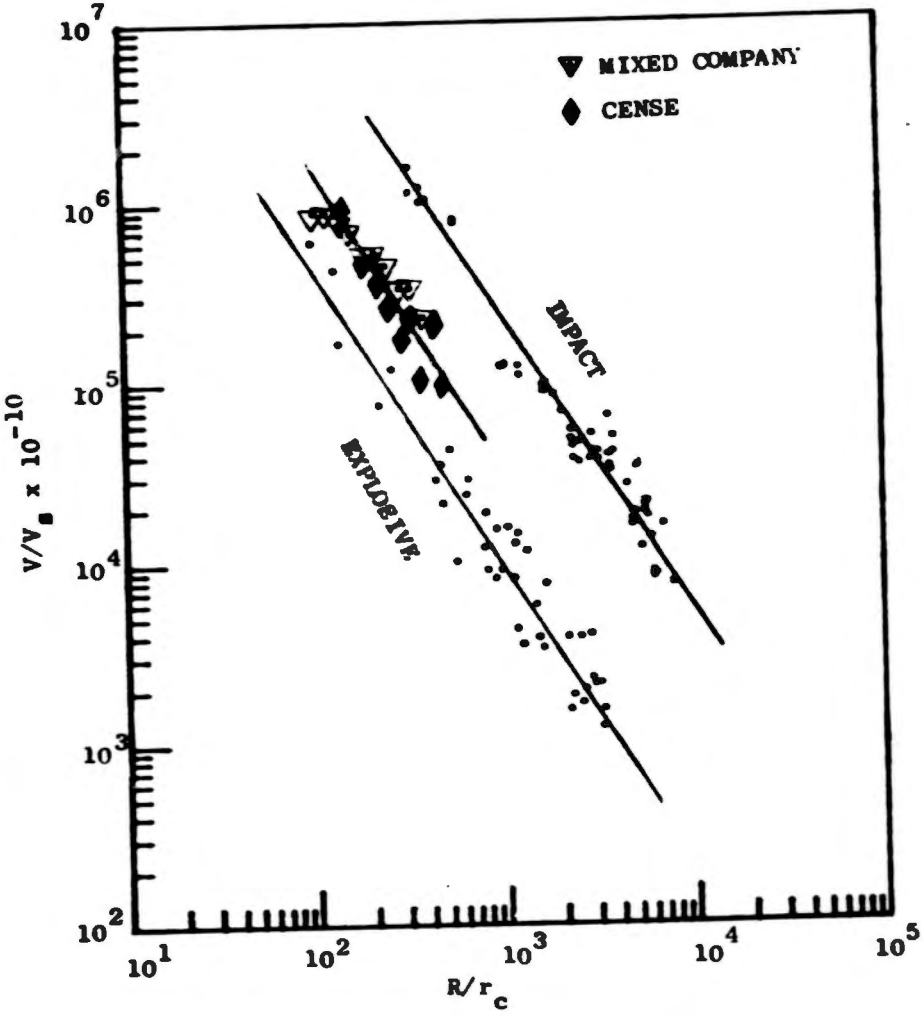

Figure 37. Normalized peak-to-peak vertical velocity as a function of scaled range

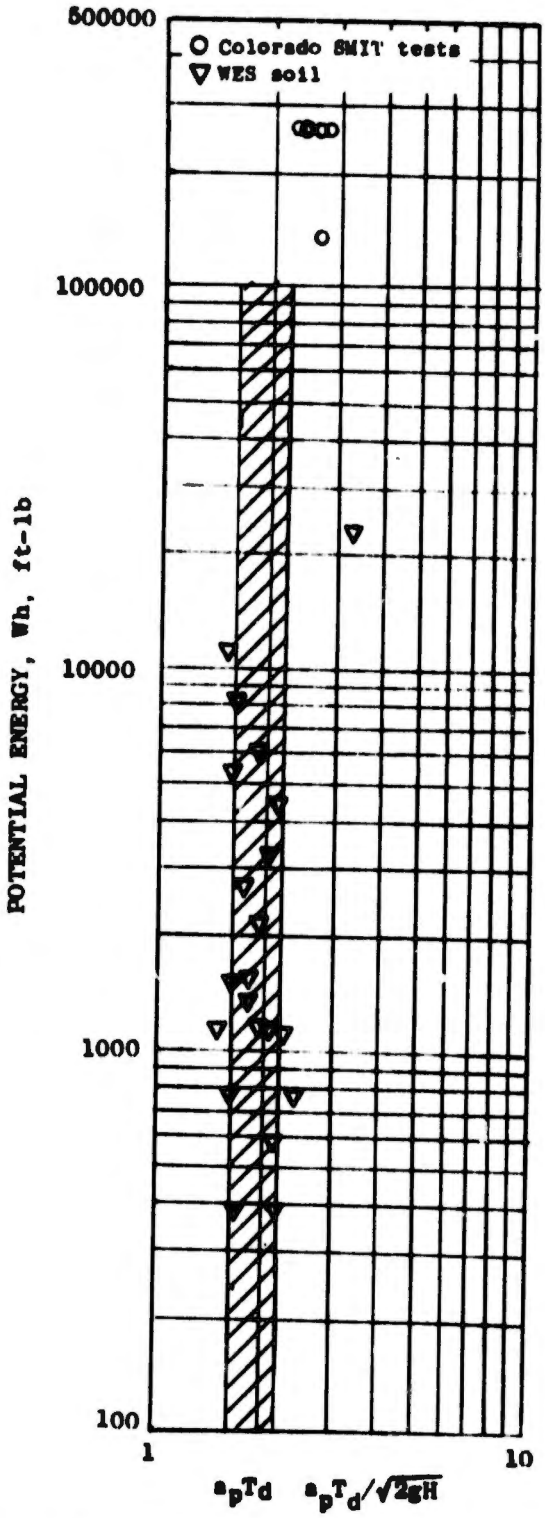

Figure 38. Normalized peak acceleration of the spheres during impact as a function of energy level

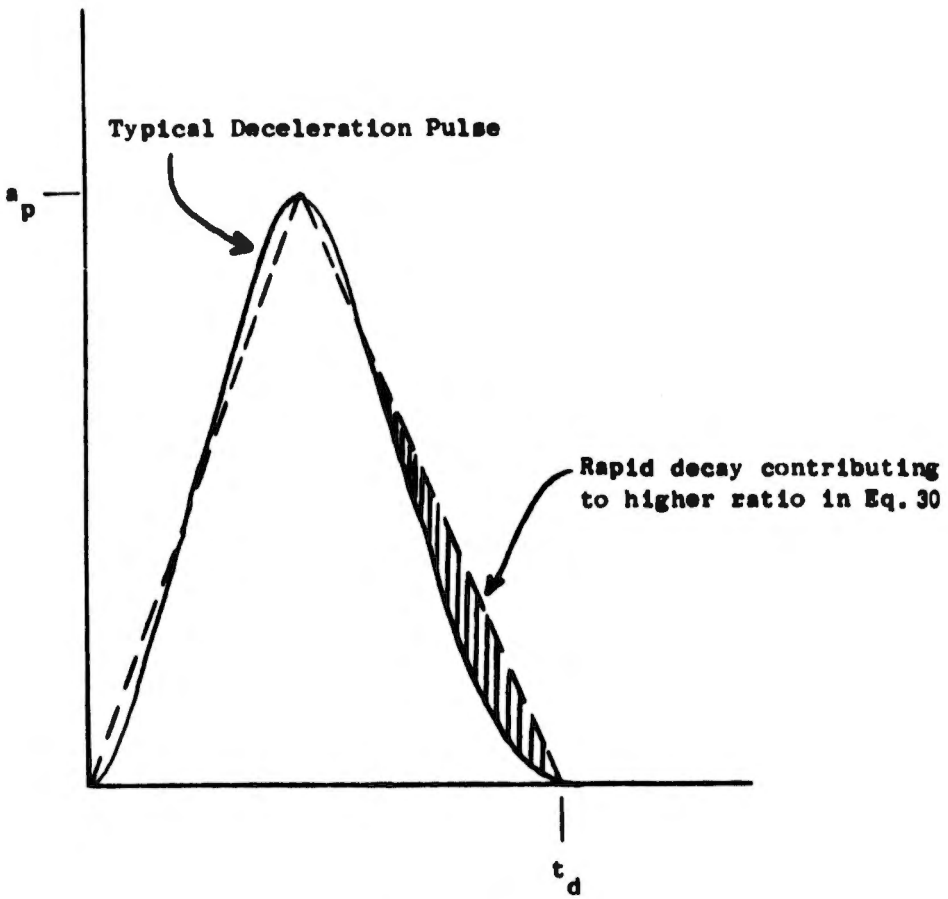

Figure 39. Typical sphere deceleration pulse compared to triangular approximation

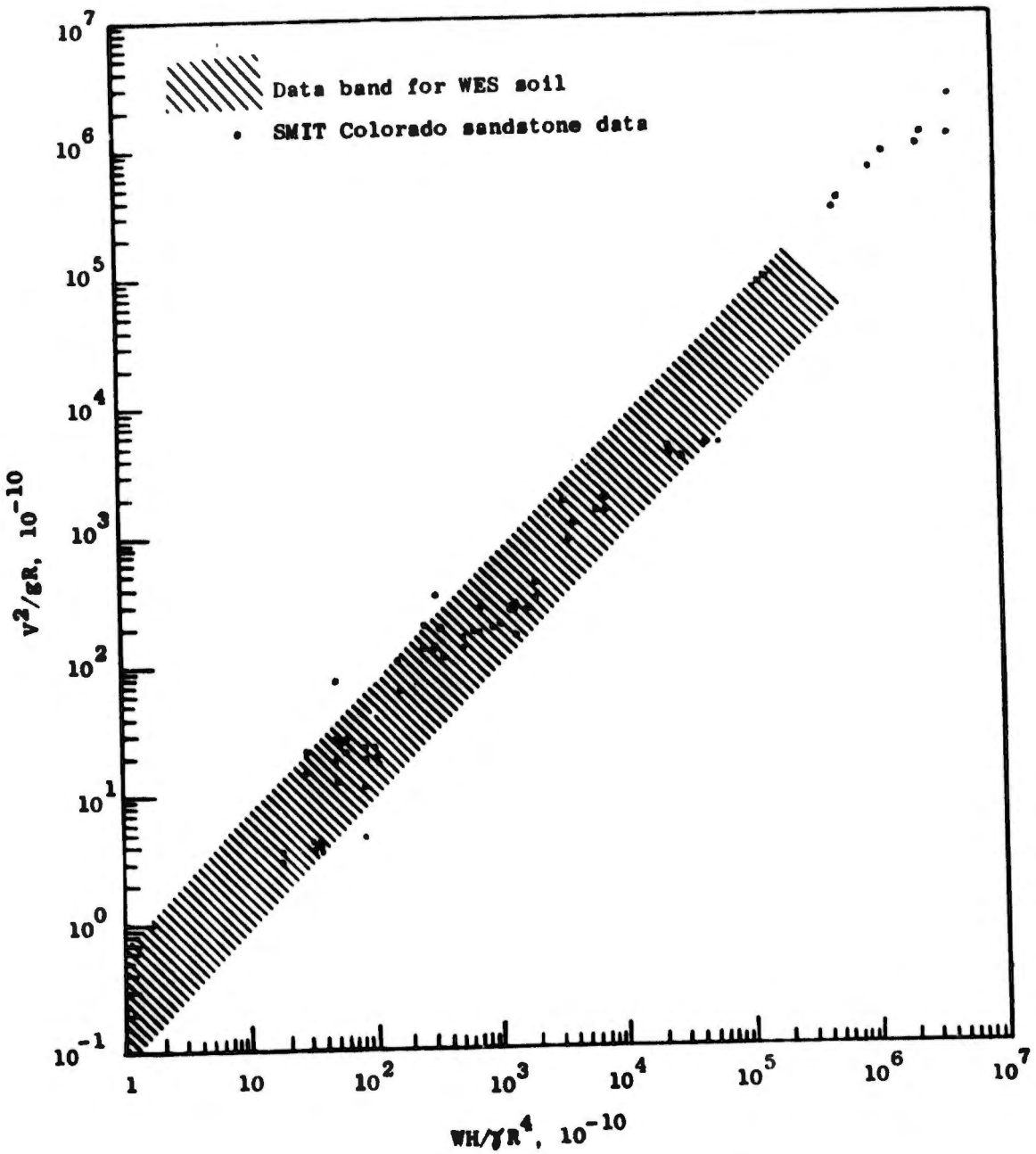

Figure 40. Normalized vertical peak particle kinetic energy as a function of normalized potential energy

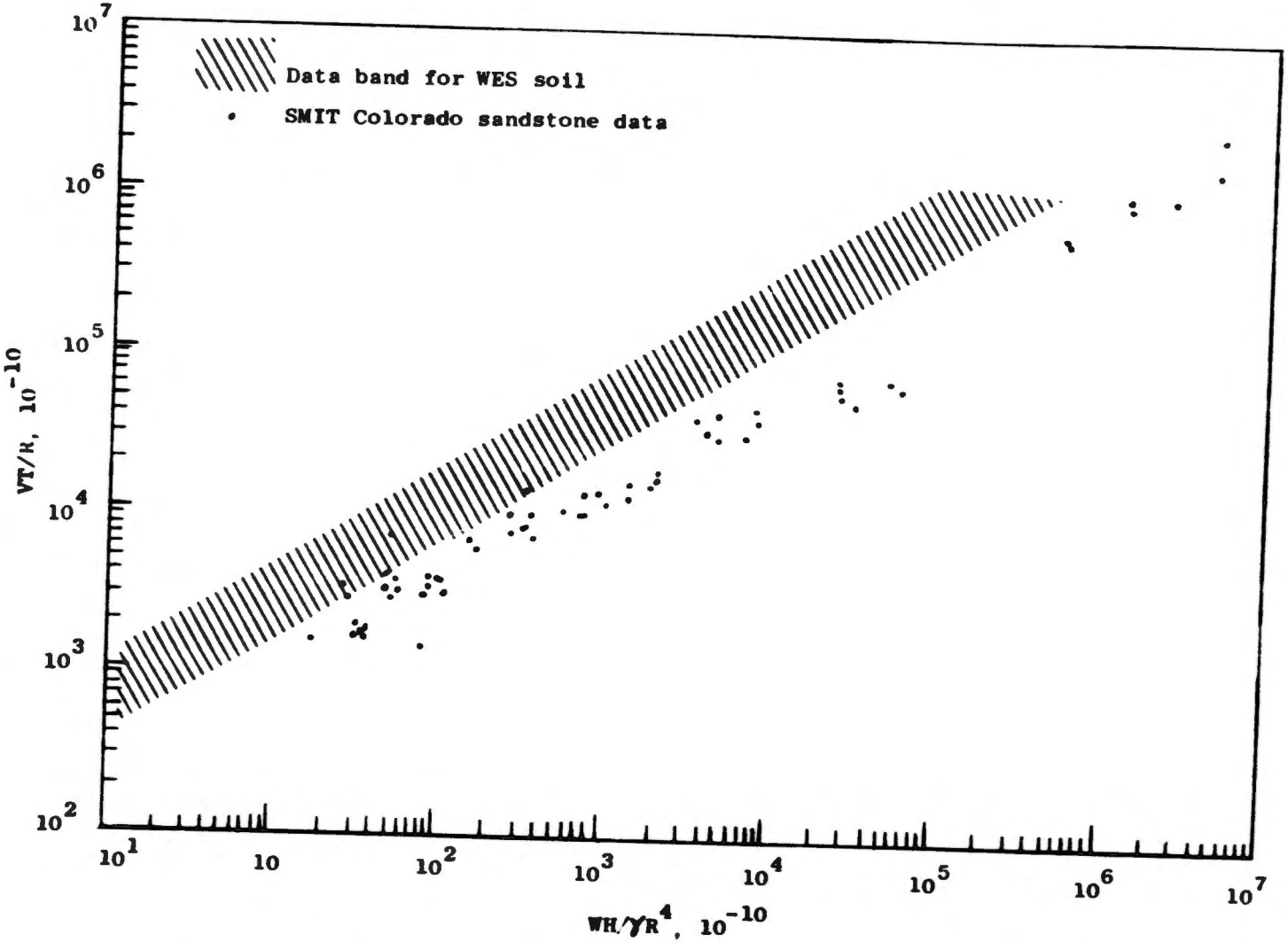

Figure 41. Normalized vertical particle displacement as a function of normalized potential energy

APPENDIX A: TESTS CONDUCTED

Explosive Tests

Type Explosive	Weight, lb	DOB, C_r	R_o, ft
Nitromethane	1000	+4	200.0
	1000	+4	200.0
	1000	+1	200.0
	1000	+1/2	225.0
	1000	0	215.0
	1000	-1/2	180.0
	1000	-1	200.0
	1000	-7	135.0
C-4	27	0	60.0
	27	-1	50.0
	18	+1	50.0
	8	+1	40.0
	8	-1/2	63.0
	4	+1/2	16.4
	4	0	28.9
	4	-1	25.5
	1	+1	14.6
	1	+1	20.0
	1	+1	32.2
	1	+1/2	14.4
	1	0	35.0
	1	0	35.0
	1	-1/2	15.0
	1	-1	35.0
	1	-1	35.2
	1	-1	35.0
	1	-1	20.0
	1	-1	20.0

Note: DOB = Depth of burst with units of charge radius.
C_r = Charge radius.
R_o = Range to the first instrument station, ft.

APPENDIX B: STATISTICALLY SIGNIFICANT CORRELATIONS FOR VERTICAL DATA

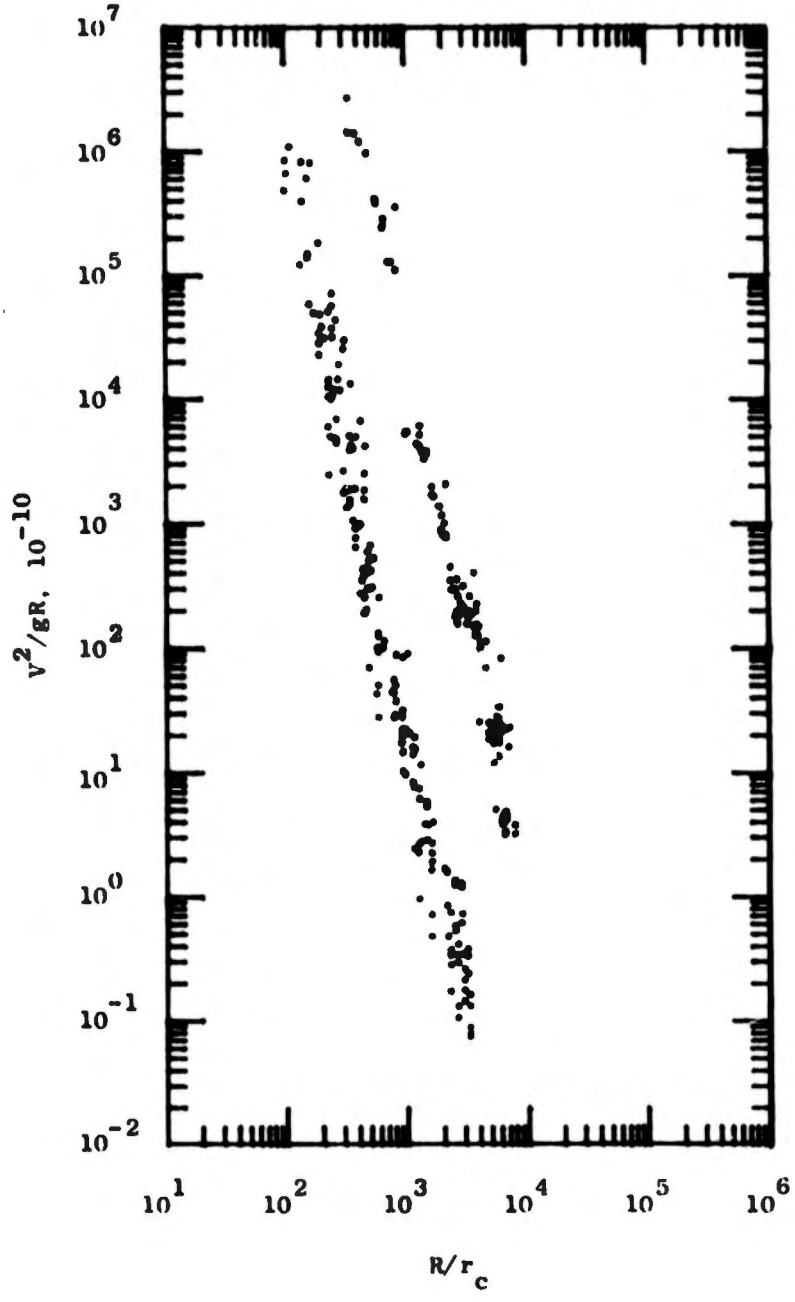
10^7
10^6
10^5
10^4
10^3
10^2
10^1
10^0
10^{-1}
10^{-2}
$V^2/gR,\ 10^{-10}$
10^1
10^2
10^3
10^4
10^5
10^6
R/r_c

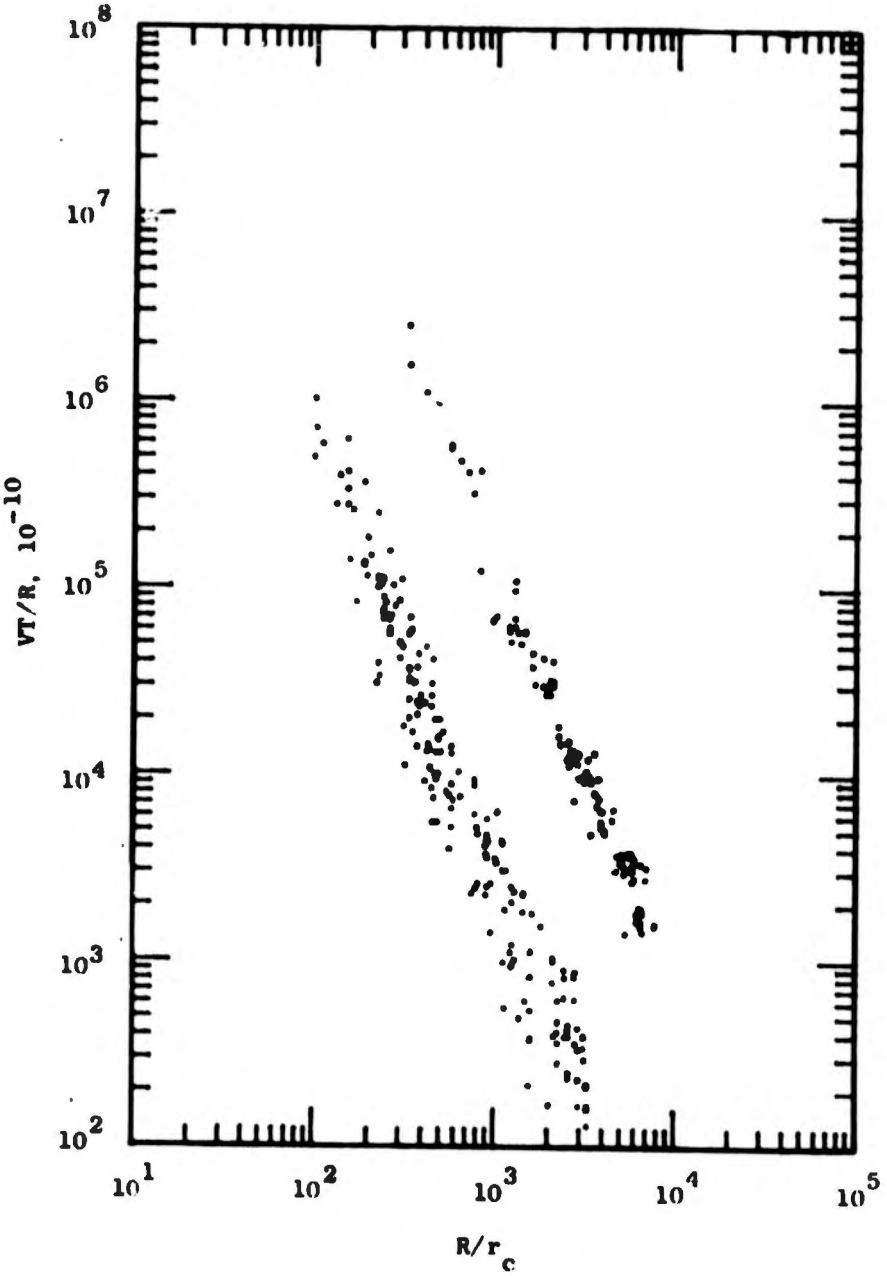
10^8
10^7
10^6
10^5
10^4
10^3
10^2
VT/R, 10^{-10}
10^1
10^2
10^3
10^4
10^5
R/r_c

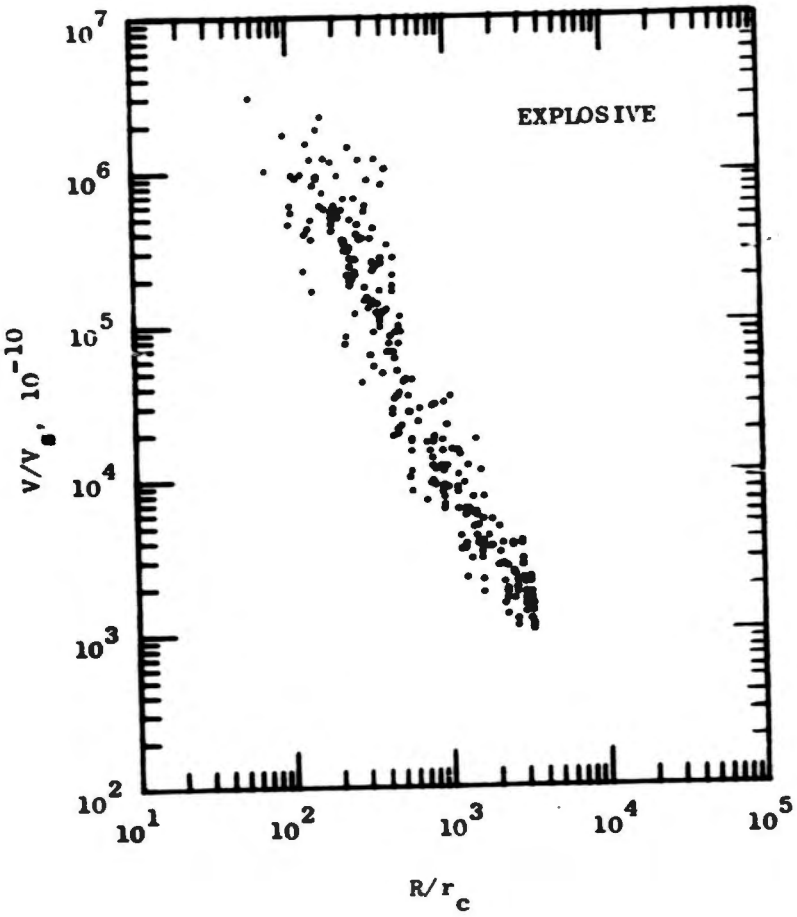
EXPLOSIVE
10^7
10^6
10^5
10^4
10^3
10^2
V/V_s, 10^{-10}
10^1
10^2
10^3
10^4
10^5
R/r_c

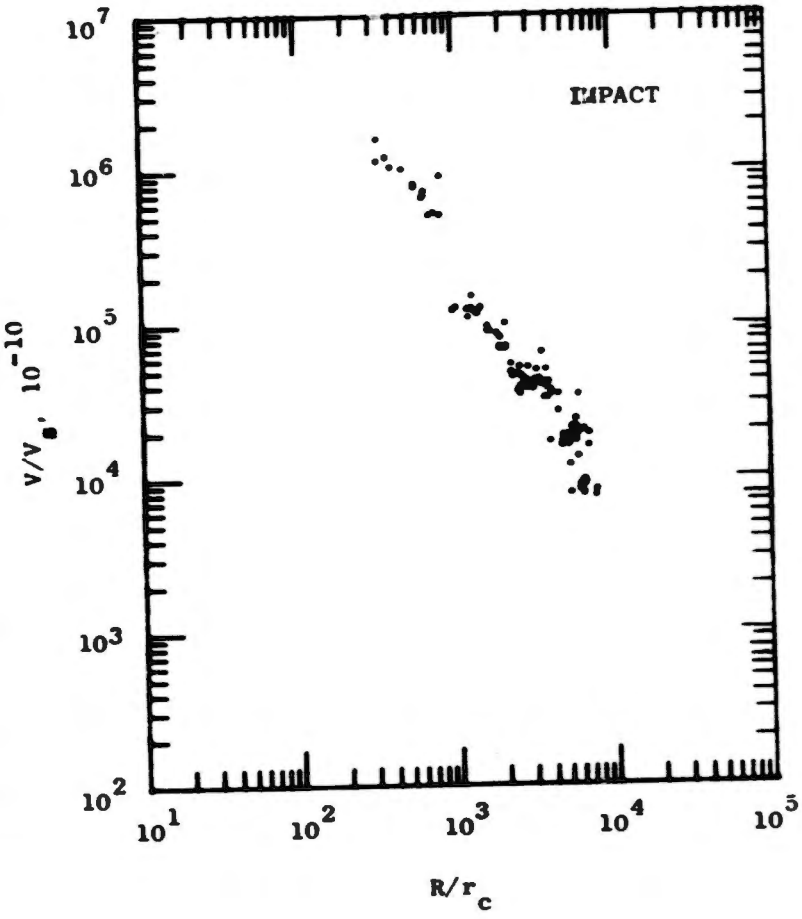
IMPACT
10^7
10^6
10^5
10^4
10^3
10^2
V/V_s, 10^{-10}
10^1
10^2
10^3
10^4
10^5
R/r_c

Crater Dimensions Associated with Spherical Mass Impact Technique

Potential Energy, E, ft-lb	Crater Radius, r_a ft	Crater Depth, d_a ft	Crater Volume, C, ft^3
136,000	0.60	0.29	0.177
272,000	0.90	0.50	0.702
272,000	0.88	0.46	0.610
272,000	0.70	0.54	0.498
272,000	0.81	0.48	0.553
272,000	0.72	0.45	0.414
272,000	0.81	0.45	0.511
272,000	0.72	0.44	0.403
272,000	0.67	0.45	0.365
272,000	0.60	0.49	0.339
272,000	0.68	0.41	0.334
272,000	0.70	0.46	0.405
272,000	0.47	0.41	0.230
272,000	0.55	0.42	0.238

APPENDIX C: CRATER DIMENSIONS

True Crater Dimensions Associated with HE Events at Various DOB's

Type Explosive	Charge Weight, W lb	Crater Radius, r_a ft	Crater Depth, d_a ft	Crater Volume,* C_v ft^3
		Surface Tangent		
NM	1000	4.4	1.7	49.0
C-4	18	1.15	0.70	1.38
C-4	8	0.9	0.63	0.76
C-4	1	0.43	0.16	0.045
C-4	1	0.43	0.30	0.083
		1/4 Buried		
NM	1000	8.9	4.2	395.0
C-4	1	0.85	0.47	0.40
		1/2 Buried		
NM	1000	9.7	4.6	680.0
C-4	27	3.2	1.65	26.5
C-4	1	1.05	0.53	0.92
C-4	1	0.87	0.5	0.59
		3/4 Buried		
NM	1000	13.5	4.6	1155.0
C-4	4	1.17	0.55	1.037
		Buried Tangent		
NM	1000	16.5	4.5	1457.0
C-4	27	4.0	1.9	36.2
	4	2.3	1.08	6.79
	1	0.31	1.0	0.114
	1	1.25	0.7	1.30
	1	1.30	0.6	1.21
	1	1.5	0.58	1.55
		Buried 7 Charge Radii		
NM	1000	23.9	12.7	6868.0

* Volumes for C-4 produced craters were approximated using crater depth and crater radius.

APPENDIX D: NOTATION

a_p Peak deceleration of sphere during impact, ft/sec^2

C_r Charge radius

C_v Crater volume, ft^3

d_a Crater depth, ft

D Depth of charge burial, center

DOB Depth of burial, charge radii

E Potential or total energy at source, ft-lb

F Force

$F(\tau)$ Force-time function

g Acceleration of gravity, 32.2 ft/sec

h Height of drop, ft

L Length

n Original number of variables

r_a Crater radius, ft

r_c Effective charge radius, ft

R Range from seismic source, ft

R_o Range to the first instrument station, ft

s Number of basic dimensions

t_d Duration of deceleration pulse, sec

T Period of dominant wave group, sec; time; Rayleigh wave period; and period of motion

V Peak-to-peak particle velocity, ft/sec

V_s Group velocity of peak surface wave, ft/sec

$\frac{V_e^2}{gR}$ Explosion-produced peak particle kinetic energy

$\frac{V_i^2}{gR}$ Impact-produced peak particle kinetic energy

$\frac{V_c T_e}{R}$ Explosion-produced peak particle displacement

$\frac{V_i T_i}{R}$ Impact-produced peak particle displacement

W Charge yield, lb-TNT

γ Mass density of the soil

In accordance with ER 70-2-3, paragraph 6c(1)(b), dated 15 February 1973, a facsimile catalog card in Library of Congress format is reproduced below.

Ford, Max B
Correlation of impact and explosively created ground shock phenomena, by Max B. Ford. Vicksburg, U. S. Army Engineer Waterways Experiment Station, 1976.
1 v. (various pagings) illus. 27 cm. (U. S. Waterways Experiment Station. Miscellaneous paper N-76-10)
Prepared for Office, Chief of Engineers, U. S. Army, Washington, D. C., under Project No. 4A061101A91D.
Includes bibliography.

1. Explosion effects. 2. Ground motion predictions. 3. Ground shock. 4. Impact. 5. Sandstones. I. U. S. Army. Corps of Engineers. (Series: U. S. Waterways Experiment Station, Vicksburg, Miss. Miscellaneous paper N-76-10)
TA7.W34m no.N-76-10